Gradient discretization of a 3D-2D-1D mixed-dimensional model with resolved interface, application to the drying of a fractured porous medium

Konstantin Brenner, Florent Chave, Roland Masson

Gradient discretization of a 3D-2D-1D mixed-dimensional model with resolved interface, application to the drying of a fractured porous medium.

K. Brenner*[1], Florent Chave†[2], and R. Masson‡[1]

[1]Université Côte d'Azur, Inria, CNRS, LJAD, Parc Valrose 06108 Nice Cedex 02, France
[1]Université Côte d'Azur, CNRS, Inria, LJAD, Parc Valrose 06108 Nice Cedex 02, France

November 12, 2021

Abstract

We consider a 3D-2D-1D mixed-dimensional diffusive model in a fractured porous medium coupling the 1D model along the centerline skeleton of a tubular network, the 2D model on a network of planar fractures and the 3D model in the surrounding matrix domain. The transmission conditions are based on a potential continuity assumption at matrix fracture interfaces, and on Robin type conditions at the resolved interfaces between the tubular network and the matrix and fracture network domains. The discretization of this mixed-dimensional model is formulated in the Gradient Discretization framework [19], which covers a large class of conforming and non conforming schemes and provides stability and error estimates based on general coercivity, consistency and limit-conformity properties. As an example of discretization fitting this framework, the mixed-dimensional version of the Vertex Approximate Gradient (VAG) scheme is developed. It is designed to allow non conforming meshes at the interface between the 1D and 3D-2D domains, to provide local flux expressions and to be asymptotic preserving in the limit of high transfer coefficients. Numerical experiments are provided on analytical solutions for simplified geometries which confirm the theoretical results. Using its equivalent Finite Volume formulation, the VAG discretization is extended to a drying mixed-dimensional model coupling the Richards equation in a fractured porous medium and the convection diffusion of the vapor molar fraction along the 1D domain. It is applied to simulate the drying process between an operating tunnel and a radioactive waste storage rock with explicit representation of the fractures in the excavated damaged zone.

Keywords: Mixed-dimensional model, Discrete Fracture Matrix model, Tubular network, Darcy flow, Drying model, Resolved interface method, Gradient Discretization, Vertex Approximate Gradient scheme, Finite Volume.

MSC2010 classification:

1 Introduction

Efficient and accurate models describing flow and transport processes in porous media with embedded tubular network systems are of utmost importance in several areas. A non ex-

*konstantin.brenner@univ-cotedazur.fr
†florent.chave@univ-cotedazur.fr
‡roland.masson@univ-cotedazur.fr

haustive list of applications includes liquid or gas flow between a well and a reservoir [27, 13], blood flow through vascularized tissue [25, 44, 48, 35, 15, 26, 37, 43], the modelling of the effect of steel components to reinforce concrete structures in civil engineering [40], the source reconstruction of electroencephalography [20], or plant root system growing in soil [31, 34, 36]. From a computational perspective, these applications are highly challenging to simulate due to the scale disparity between the tubular and the surrounding domains.

To partially overcome this complexity, a reduction of dimension is usually performed for tubular networks with large longitudinal dimension compared with their section size. It leads to mixed-dimensional models coupling the 1D reduced model along the centerline skeleton of the tubular network to the 3D model in the embedding bulk domain. Such mixed-dimensional models differ in the way the coupling terms are modelled at the interface Γ between the tubular network and the embedding bulk domain, based on transfer coefficients. Implicit interface methods do not resolve the interface Γ and approximate the coupling terms either as a line source [29, 15, 14, 12, 28, 5], a surface source [38, 39] or a volumetric source [35]. These type of methods allow a simple meshing procedure of the bulk domain possibly independent of the tubular network. They are adapted to highly complex networks but can suffer from approximation errors in case of high gradients at the interface. On the other hand explicit interface methods require to build a mesh resolving the interface but include fewer modelling assumptions and can capture highly nonlinear behavior at the interface [33].

This work focuses on explicit interface methods [33]. This is motivated by our application to drying processes at the interface between operating tunnels and radioactive waste storage requiring a high resolution at a scale much smaller than the tunnel radius to capture accurately the liquid pressure gradient [10]. This application also motivates to take into account a network of fractures in the so-called excavated damaged zone (EDZ) at the interface between the tunnel and the porous storage rock. We consider the reduced model for which the fractures are represented as interfaces of codimension one immersed in the surrounding matrix domain. To fix ideas, the solution is considered continuous at matrix fracture interfaces assuming that the fractures act as drains [1, 2, 6, 45, 7] as opposed to discontinuous models at matrix fracture interfaces for fractures acting either as drains or barriers [24, 30, 3, 8, 32, 42].

This leads to a mixed-dimensional model coupling the 3D model in the matrix, the 2D model in the fracture network and the 1D model along the centerline skeleton. In order to simplify the presentation and focus on the difficulties raised by the coupling with the fractures, we consider in what follows a domain defined by an hollow cylinder with a single cylindrical tube and a network of planar fractures. Note however that the framework and discretization investigated in this work readily extend to more complex domains and tubular networks provided that a surjective mapping from the interface Γ to the 1D centerline skeleton is defined; see [33] and references therein.

The core of this work deals with the mixed-dimensional 3D-2D-1D diffusive model. We first define the functional setting including the potential and the flux function spaces and we state density results for their respective smooth function subspaces that will be used for the subsequent numerical analysis. A key difficulty of this functional analysis framework is related to the intersections between the fractures and the interface Γ. Then, the Gradient Discretization (GD) of the mixed-dimensional model is defined. This framework introduced in [19] is based on abstract vector spaces of discrete unknowns as well as on abstract reconstruction operators for the functions and their gradients. Based on general coercivity, consistency and limit conformity properties, it derives stability and error estimates for the discrete variational approximation of the model. Note that the GD framework accounts for

both conforming and non conforming approximations, which is a key feature in order to include separate meshes for the porous and tubular domains.

As an example of GD, the 3D-2D-1D mixed-dimensional version of the Vertex Approximate Gradient (VAG) scheme is then derived. The VAG scheme was introduced in [23] for single phase Darcy flow and in [7, 8] for mixed-dimensional Darcy flow in fractured media. The VAG scheme is roughly speaking a finite volume nodal approximation. Its main advantage compared with typical nodal finite volume schemes such as Control Volume Finite Element (CVFE) methods [4] is to avoid the mixing of different material properties inside the control volumes. This idea is here extended to take into account the coupling with the 1D domain using a 1D finite element mesh non necessarily matching with the porous medium mesh. The coupling terms at the interface Γ between the 1D domain and both the matrix and the fractures are discretized based on a simple interpolation operator. It is designed to provide local flux expressions, leading to an easy extension to more complex physics such as drying models and to preserve optimal convergence rates. It is also shown to be asymptotic preserving in the limit of large (convective) transfer coefficients. This mixed-dimensional VAG scheme is shown to meet the GD properties and to provide first order error estimates on piece-wise smooth solutions. These theoretical results are investigated numerically based on analytical solutions built on a simplified geometry including a single fracture either parallel or perpendicular to the 1D domain axis. Finally, the VAG discretization is extended to a simplified drying model coupling the Richards equation in a fractured porous medium with the convective diffusion of the vapor molar fraction along the tunnel.

The material is organized as follows. In Section 2, we introduce the continuous setting and describe the equations that govern the mixed-dimensional model along with its weak formulation. In Section 3 we introduce the discrete setting in the GD framework. In Section 4, we formulate the VAG approximation. Section 4.4 contains the main theoretical results of the VAG discretization and Section 5 contains an extensive numerical validation of the method as well as its application to a nonlinear drying model. Finally, Section 7 is dedicated to the proofs of theoretical results stated in Sections 3 and 4.4. Readers mainly interested in the numerical recipe and results can skip this section at first reading.

2 The mixed-dimensional model

In this section, we introduce the strong and the weak formulations of the reduced model, preceded by notation and functional settings.

2.1 Geometry settings

The computational domain represents an excavated tunnel imbedded in a fractured porous medium. To simplify the notations and focus on the difficulties raised by the fracture network, the porous geometrical domain is assumed to be an hollow cylinder (see Figure 1). From a mathematical viewpoint, let ω and $\omega_g \subset \omega$ be two open, bounded, simply connected polygonal sets of $\mathbb{R}^2$ with Lipschitz boundaries and $L > 0$ be the excavation length. The porous medium can be seen as a cylindrical domain $\Omega_p := (0, L) \times (\omega \setminus \overline{\omega_g})$ with an axial hole $(0, L) \times \omega_g$ corresponding to the excavated tunnel, along the x-axis for simplicity. The axis of the tunnel is denoted by $\Omega_g = (0, L) \times \{\boldsymbol{x}_g\}$, with $\boldsymbol{x}_g$ the center of gravity of ω_g to fix ideas. The porous medium Ω_p contains a fracture network Ω_f, with $\overline{\Omega_f} = \bigcup_{i \in \mathcal{I}_f} \overline{\Omega_{f,i}}$ where for all $i \in \mathcal{I}_f$, $\Omega_{f,i} \subset \Omega_p$ is an open, bounded, simply connected polygonal set included in a plane $\mathcal{P}_i$ of $\mathbb{R}^3$. For all $i, j \in \mathcal{I}_f$, $i \neq j$, we assume that the angles of $\Omega_{f,i}$ are strictly smaller than 2π,

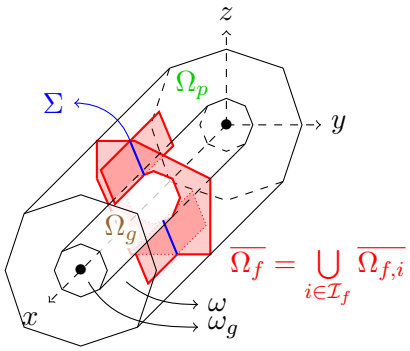

Figure 1: Illustration of the notations introduced in Section 2.1. with the 3D porous medium domain Ω_p, the 2D fracture network Ω_f and the 1D axis Ω_g of the excavated tunnel.

that $\Omega_{f,i} \cap \overline{\Omega_{f,j}} = \emptyset$ and that $\Omega_f \cap \partial\Omega_p = \emptyset$. The matrix domain is denoted by $\Omega_m := \Omega_p \setminus \overline{\Omega_f}$. The interface between the tunnel and the porous medium is denoted by $\Gamma := (0, L) \times \partial\omega_g$. We assume that Dirichlet boundary conditions are imposed on $\Gamma_D := \partial\Omega_p \setminus \overline{\Gamma}$. Concerning the fracture network boundaries, let us set

$$\begin{cases} \Sigma_\Gamma := \partial\Omega_f \cap \Gamma, \\ \Sigma_D := \partial\Omega_f \cap \Gamma_D, \\ \Sigma_N := \partial\Omega_f \setminus \overline{\Sigma_\Gamma \cup \Sigma_D}, \end{cases}$$

and let us also denote by Σ the fracture intersections excluding Σ_Γ and Σ_D (see Figure 1).

The tunnel axis Ω_g is readily parametrized in the following by $x \in (0, L)$. It results that a surjective mapping from Γ to Ω_g is implicitly defined in what follows by the x coordinate. Note that an explicit definition of such surjective mapping is the key ingredient in order to extend the framework to more complex geometries (see e.g. [33]).

2.2 Functional settings

We denote by $H^1(\Omega_f)$ the function space of scalar functions on Ω_f whose restriction to $\Omega_{f,i}$, $i \in \mathcal{I}_f$, is in $H^1(\Omega_{f,i})$ and whose traces on fracture intersections are continuous. We define the trace operators $\gamma_f : H^1(\Omega_p) \to L^2(\Omega_f)$ and $\gamma_\Gamma : H^1(\Omega_p) \to L^2(\Gamma)$, together with the trace operators from $H^1(\Omega_f)$ to $L^2(\Sigma_\Gamma)$ and $H^1(\Gamma)$ to $L^2(\Sigma_\Gamma)$, both denoted by γ_{Σ_Γ} for convenience. We also define the function space in the porous domain Ω_p and its associated subspace taking into account homogeneous Dirichlet boundary conditions on Γ_D and Σ_D as

$$V^p := \{v_p \in H^1(\Omega_p) \,|\, \gamma_f v_p \in H^1(\Omega_f)\}, \quad V_0^p := \{v_p \in V \,|\, v_p = 0 \text{ on } \Gamma_D,\ \gamma_f v_p = 0 \text{ on } \Sigma_D\}.$$

The global function space together with its subpace enforcing strongly the homogeneous Dirichlet boundary conditions are then defined by

$$V := V^p \times H^1(\Omega_g), \quad V_0 := V_0^p \times H_0^1(\Omega_g).$$

For any $v = (v_p, v_g) \in V$, the jump operators across Γ and Σ_Γ are denoted by

$$[\![v]\!]_\Gamma := \gamma_\Gamma v_p - v_g \in L^2(\Gamma), \qquad [\![v]\!]_{\Sigma_\Gamma} := \gamma_{\Sigma_\Gamma}\gamma_f v_p - v_g \in L^2(\Sigma_\Gamma), \tag{1}$$

where v_g is implicitely extended to Γ (resp. Σ_Γ) using the x coordinate mapping from Γ to Ω_g (resp. from Σ_Γ to Ω_g).

Denoting by ∇_τ the tangential gradient operator, we equip the space V with the following seminorm

$$\|v\|_V^2 \coloneqq \int_{\Omega_m} |\nabla v_p(\boldsymbol{x})|^2 \mathrm{d}\boldsymbol{x} + \int_{\Omega_f} |\nabla_\tau \gamma_f v_p(\boldsymbol{x})|^2 \mathrm{d}\tau(\boldsymbol{x}) + \int_\Gamma [\![v]\!]_\Gamma^2(\boldsymbol{x}) \mathrm{d}\tau(\boldsymbol{x}) + \int_{\Sigma_\Gamma} [\![v]\!]_{\Sigma_\Gamma}^2(\boldsymbol{x}) dl(\boldsymbol{x}) + \int_{\Omega_g} |v_g'|^2 \mathrm{d}x.$$

We can readily prove the following proposition which extends to more general boundary conditions than the one considered here.

Proposition 2.1 (Norm $\|\cdot\|_V$)**.** *The functional $\|\cdot\|_V$ defines a norm on V_0*

The following density result has been proved in [7, Proposition 2].

Lemma 2.1. *The function space defined by $C^\infty_{V_0^p} \coloneqq C^\infty(\overline{\Omega_p}) \cap V_0^p$ is a dense subspace of V_0^p endowed with the norm $\left(\int_{\Omega_m} |\nabla v_p(\boldsymbol{x})|^2 \mathrm{d}\boldsymbol{x} + \int_{\Omega_f} |\nabla_\tau \gamma_f v_p(\boldsymbol{x})|^2 \mathrm{d}\tau(\boldsymbol{x})\right)^{\frac{1}{2}}$.*

We now define the function space for the porous medium fluxes

$$W^p \coloneqq \left\{ \begin{array}{l} \boldsymbol{q}_p = (\boldsymbol{q}_m, \boldsymbol{q}_f) \in H(\mathrm{div}; \Omega_m) \times L^2(\Omega_f)^2 \mid (\boldsymbol{q}_m \cdot \boldsymbol{n}_\Gamma)_{|\Gamma} \in L^2(\Gamma), \\ (\boldsymbol{q}_f \cdot \boldsymbol{n}_{\Sigma_\Gamma})_{|\Sigma_\Gamma} \in L^2(\Sigma_\Gamma) \text{ and there exists } r_f(\boldsymbol{q}_p) \in L^2(\Omega_f) \text{ such that} \\ \displaystyle\int_{\Omega_m} (\boldsymbol{q}_m \cdot \nabla v + v\ \mathrm{div}(\boldsymbol{q}_m)) \mathrm{d}\boldsymbol{x} + \int_{\Omega_f} (\boldsymbol{q}_f \cdot \nabla_\tau \gamma_f v + r_f(\boldsymbol{q}_p) \gamma_f v) \mathrm{d}\tau(\boldsymbol{x}) \\ \displaystyle - \int_\Gamma (\boldsymbol{q}_m \cdot \boldsymbol{n}_\Gamma) \gamma_\Gamma v\ \mathrm{d}\tau(\boldsymbol{x}) - \int_{\Sigma_\Gamma} (\boldsymbol{q}_f \cdot \boldsymbol{n}_{\Sigma_\Gamma}) \gamma_{\Sigma_\Gamma} v\ \mathrm{d}l(\boldsymbol{x}) = 0 \text{ for all } v \in V_0^p \end{array} \right\}, \quad (2)$$

and the flux space for the mixed-dimensional diffusion model

$$W \coloneqq \left\{ \begin{array}{l} \boldsymbol{q} = (\boldsymbol{q}_p, q_g) \in W^p \times L^2(\Omega_g) \mid \text{there exists } r_g(\boldsymbol{q}) \in L^2(\Omega_g) \text{ such that} \\ \displaystyle\int_\Gamma (\boldsymbol{q}_m \cdot \boldsymbol{n}_\Gamma) v_g(x) \mathrm{d}\tau(\boldsymbol{x}) + \int_{\Sigma_\Gamma} (\boldsymbol{q}_f \cdot \boldsymbol{n}_{\Sigma_\Gamma}) v_g(x) \mathrm{d}l(\boldsymbol{x}) \\ \displaystyle + \int_{\Omega_g} (q_g v_g' + r_g(\boldsymbol{q}) v_g) \mathrm{d}x = 0 \text{ for all } v_g \in H_0^1(\Omega_g) \end{array} \right\}, \quad (3)$$

where $\boldsymbol{n}_\Gamma$ (resp. $\boldsymbol{n}_{\Sigma_\Gamma}$) is the unit normal vector to Γ (resp. Σ_Γ) oriented outward to Ω_m (resp. Ω_f). In the definition (3) of the space W, the uniqueness of $r_g(\boldsymbol{q})$ is clear and the uniqueness of $r_f(\boldsymbol{q}_p)$ is obtained using liftings from the function space $C_c^\infty(\Omega_{f,i})$ to the function space $C^\infty_{V_0^p}$ for all $i \in \mathcal{I}_f$. The function space W is an Hilbert space endowed with the following scalar product: for all $(\boldsymbol{p}, \boldsymbol{q}) \in W \times W$

$$\begin{aligned} \langle \boldsymbol{p}, \boldsymbol{q} \rangle_W \coloneqq & \int_{\Omega_m} (\boldsymbol{p}_m \cdot \boldsymbol{q}_m + \mathrm{div}(\boldsymbol{p}_m) \mathrm{div}(\boldsymbol{q}_m))\, \mathrm{d}\boldsymbol{x} \\ & + \int_{\Omega_f} \left(\boldsymbol{p}_f \cdot \boldsymbol{q}_f + r_f(\boldsymbol{p}_p) r_f(\boldsymbol{q}_p)\right) \mathrm{d}\tau(\boldsymbol{x}) + \int_{\Omega_g} (p_g q_g + r_g(\boldsymbol{p}) r_g(\boldsymbol{q}))\, \mathrm{d}x \\ & + \int_\Gamma (\boldsymbol{p}_m \cdot \boldsymbol{n}_\Gamma)(\boldsymbol{q}_m \cdot \boldsymbol{n}_\Gamma) \mathrm{d}\tau(\boldsymbol{x}) + \int_{\Sigma_\Gamma} (\boldsymbol{p}_f \cdot \boldsymbol{n}_{\Sigma_\Gamma})(\boldsymbol{q}_f \cdot \boldsymbol{n}_{\Sigma_\Gamma}) \mathrm{d}l(\boldsymbol{x}). \end{aligned} \quad (4)$$

Note that the definition (3) of the space W incorporates the physical assumption that the sum of the normal fluxes at fracture intersections Σ as well as the normal flux at the immersed fracture boundary Σ_N vanish.

We now define a subspace of smooth functions in W. Let us denote by $(\hat{x}_k)_{k\in S_{\Sigma_\Gamma}}$ the sequence of points $\hat{x}_k \in \Omega_g$ such that the one-dimensional measure of the set $(\{\hat{x}_k\}\times\partial\omega_g)\cap\Sigma_\Gamma$ is nonzero, and for all $k \in S_{\Sigma_\Gamma}$, by $H_k(\cdot)$ the Heaviside step function on Ω_g such that $H_k(x) = 0$ if $x < \hat{x}_k$ and $H_k(x) = 1$ otherwise. Then, we set

$$C_W^\infty \coloneqq \left\{ \begin{array}{l} (\boldsymbol{q}_m, \boldsymbol{q}_f, q_g) \mid \boldsymbol{q}_m \in C^\infty(\overline{\Omega}_m)^3,\ \boldsymbol{q}_f \in C^\infty(\overline{\Omega}_f)^2, \\ q_g - \displaystyle\sum_{k\in S_{\Sigma_\Gamma}} \left(\int_{(\{\hat{x}_k\}\times\partial\omega_g)\cap\Sigma_\Gamma} \boldsymbol{q}_f\cdot\boldsymbol{n}_{\Sigma_\Gamma}\mathrm{d}l(\boldsymbol{x}) \right) H_k(x) \in C^\infty(\overline{\Omega}_g) \end{array} \right\}. \tag{5}$$

Here $C^\infty(\overline{\Omega}_m)^3$ is the space of smooth functions $\Omega_m \to \mathbb{R}^3$ whose derivatives of any order admit finite limits on both sides of Ω_f, and $C^\infty(\overline{\Omega}_f)^2$ is the space of functions whose restrictions to each $\Omega_{f,i}$ is in $C^\infty(\overline{\Omega}_{f,i})^2$ tangent to $\Omega_{f,i}$ and satisfying normal flux conservation at Σ and vanishing normal flux at Σ_N.

Lemma 2.2. *The function space C_W^∞ is a dense subspace of W.*

Proof. See Section 7.1. □

2.3 Model problem

In the matrix domain Ω_m (resp. fracture network Ω_f), we denote by $\boldsymbol{\Lambda}_m \in L^\infty(\Omega_p)^{3\times3}$ (resp. $\boldsymbol{\Lambda}_f \in L^\infty(\Omega_f)^{2\times2}$) the diffusion tensor (resp. tangential diffusion tensor) and assume that there exist $\overline{\lambda}_m \geq \underline{\lambda}_m > 0$ (resp. $\overline{\lambda}_f \geq \underline{\lambda}_f > 0$) such that

$$\underline{\lambda}_m|\boldsymbol{\xi}|^2 \leq \boldsymbol{\Lambda}_m(\boldsymbol{x})\boldsymbol{\xi}\cdot\boldsymbol{\xi} \leq \overline{\lambda}_m|\boldsymbol{\xi}|^2 \text{ for all } \boldsymbol{\xi}\in\mathbb{R}^3 \text{ and for a.e. } \boldsymbol{x}\in\Omega_p,$$

(resp. $\underline{\lambda}_f|\boldsymbol{\xi}|^2 \leq \boldsymbol{\Lambda}_f(\boldsymbol{x})\boldsymbol{\xi}\cdot\boldsymbol{\xi} \leq \overline{\lambda}_f|\boldsymbol{\xi}|^2$ for all $\boldsymbol{\xi}\in\mathbb{R}^2$ and for a.e. $\boldsymbol{x}\in\Omega_f$). On the tunnel side, we denote by $\Lambda_g \in L^\infty(\Omega_g)$ the longitudinal diffusion coefficient in the tunnel and assume that $\underline{\lambda}_g \leq \Lambda_g(x) \leq \overline{\lambda}_g$ for a.e. $x \in \Omega_g$ with $\overline{\lambda}_g \geq \underline{\lambda}_g > 0$ two positive constants. We denote by $d_f \in L^\infty(\Omega_f)$ the width of the fractures, assumed to be such that $\underline{d}_f \leq d_f(\boldsymbol{x}) \leq \overline{d}_f$ for a.e. $\boldsymbol{x}\in\Omega_f$ with $\overline{d}_f \geq \underline{d}_f > 0$ two positive constants. The transfer coefficient at the interface Γ is denoted by $H_g \in L^\infty(\Gamma)$ and is assumed to verify $\underline{H}_g \leq H_g(\boldsymbol{x}) \leq \overline{H}_g$ for a.e. $\boldsymbol{x}\in\Gamma$ with $\overline{H}_g \geq \underline{H}_g > 0$ two positive constants.

We consider the following mixed dimensional linear diffusion model that consists in seeking $u = (u_p, u_g) \in V_0$ and $\boldsymbol{q} = (\boldsymbol{q}_p, q_g) \in W$ such that

$$\left\{ \begin{array}{rll} \mathrm{div}(\boldsymbol{q}_m) = \mathrm{f}_m & & \text{in } \Omega_m, \\ r_f(\boldsymbol{q}_p) = d_f\mathrm{f}_f & & \text{in } \Omega_f, \\ r_g(\boldsymbol{q}) = |\omega_g|\mathrm{f}_g & & \text{in } \Omega_g, \\ \boldsymbol{q}_m = -\boldsymbol{\Lambda}_m\nabla u_p & & \text{in } \Omega_m, \\ \boldsymbol{q}_f = -d_f\boldsymbol{\Lambda}_f\nabla_\tau\gamma_f u_p & & \text{in } \Omega_f, \\ q_g = -|\omega_g|\Lambda_g u_g' & & \text{in } \Omega_g, \end{array} \right. \tag{6}$$

with $\mathrm{f}_m \in L^2(\Omega_p)$, $\mathrm{f}_f \in L^2(\Omega_f)$, and $\mathrm{f}_g \in L^2(\Omega_g)$ denoting the source terms in the matrix, the fracture network and the tunnel, respectively. The problem (6) is closed by the following interface conditions

$$\left\{ \begin{array}{ll} \boldsymbol{q}_m\cdot\boldsymbol{n}_\Gamma = H_g[\![u]\!]_\Gamma & \text{on } \Gamma, \\ \boldsymbol{q}_f\cdot\boldsymbol{n}_{\Sigma_\Gamma} = d_f H_g[\![u]\!]_{\Sigma_\Gamma} & \text{on } \Sigma_\Gamma, \end{array} \right. \tag{7}$$

relating the jumps of the potential at the interface to the porous medium fluxes.

Remark 2.1 (Continuous model at the porous medium-tunnel interface as a limit case)**.** *We notice that in the limit case $H_g \to +\infty$, the transmission conditions (7) reduce to*

$$\begin{cases} [\![u]\!]_\Gamma = 0 & \text{on } \Gamma, \\ [\![u]\!]_{\Sigma_\Gamma} = 0 & \text{on } \Sigma_\Gamma, \end{cases} \tag{8}$$

and recalling the definition (1) of the jump operators $[\![\cdot]\!]_\Gamma$ and $[\![\cdot]\!]_{\Sigma_\Gamma}$, we obtain $\gamma_\Gamma u_p = u_g$ on Γ and $\gamma_{\Sigma_\Gamma}\gamma_f u_p = u_g$ on Σ_Γ corresponding to the continuity assumption at the porous medium-tunnel interface. This is for instance a typical assumption for the gas pressure when considering a gas free flow model along the tunnel.

The weak formulation of (6)-(7) amounts to find $u = (u_p, u_g) \in V_0$ such that

$$\begin{aligned} &\int_{\Omega_m} \mathbf{\Lambda}_m \nabla u_p \cdot \nabla v_p \mathrm{d}\boldsymbol{x} + \int_{\Omega_f} d_f \mathbf{\Lambda}_f \nabla_\tau \gamma_f u_p \cdot \nabla_\tau \gamma_f v_p \mathrm{d}\tau(\boldsymbol{x}) + \int_{\Omega_g} |\omega_g| \Lambda_g u_g' v_g' \mathrm{d}x \\ &\quad + \int_\Gamma H_g [\![u]\!]_\Gamma [\![v]\!]_\Gamma \mathrm{d}\tau(\boldsymbol{x}) + \int_{\Sigma_\Gamma} d_f H_g [\![u]\!]_{\Sigma_\Gamma} [\![v]\!]_{\Sigma_\Gamma} \mathrm{d}l(\boldsymbol{x}) \\ &\qquad = \int_{\Omega_m} \mathrm{f}_m v_p \mathrm{d}\boldsymbol{x} + \int_{\Omega_f} d_f \mathrm{f}_f \ \gamma_f v_p \mathrm{d}\tau(\boldsymbol{x}) + \int_{\Omega_g} |\omega_g| \mathrm{f}_g v_g \mathrm{d}x, \end{aligned} \tag{9}$$

for all $v = (v_p, v_g) \in V_0$. The existence and uniqueness of a solution to (9) follows from Proposition 2.1 and the Lax Milgram theorem.

3 Gradient Discretization Method

In what follows, for a given domain X of dimension d, we denote by $\|\cdot\|_X$ the usual inner norm on $L^2(X)^l$ for $l \in \{1, d\}$ without ambiguity.

3.1 Discrete general settings

The gradient discretization $\mathcal{D}$ for the model problem (9) is defined by a vector space of degrees of freedom $X_\mathcal{D} = X_{\mathcal{D}_p} \times X_{\mathcal{D}_g}$, its subspace strongly enforcing homogeneous Dirichlet boundary conditions $X_\mathcal{D}^0$, and the following set of linear operators: (i) three function reconstruction operators: $\Pi_{\mathcal{D}_m} : X_{\mathcal{D}_p} \to L^2(\Omega_p)$, $\Pi_{\mathcal{D}_f} : X_{\mathcal{D}_p} \to L^2(\Omega_f)$ and $\Pi_{\mathcal{D}_g} : X_{\mathcal{D}_g} \to L^2(\Omega_g)$, (ii) three discrete gradient reconstruction operators: $\nabla_{\mathcal{D}_m} : X_{\mathcal{D}_p} \to L^2(\Omega_p)^3$, $\nabla_{\mathcal{D}_f} : X_{\mathcal{D}_p} \to L^2(\Omega_f)^2$ and $\nabla_{\mathcal{D}_g} : X_{\mathcal{D}_g} \to L^2(\Omega_g)$, and (iii) two jump reconstruction operators: $[\![\cdot]\!]_{\mathcal{D},\Gamma} : X_\mathcal{D} \to L^2(\Gamma)$ and $[\![\cdot]\!]_{\mathcal{D},\Sigma_\Gamma} : X_\mathcal{D} \to L^2(\Sigma_\Gamma)$. The vector space $X_\mathcal{D}$ is endowed with the seminorm

$$\|v_\mathcal{D}\|_\mathcal{D}^2 \coloneqq \|\nabla_{\mathcal{D}_m} v_{\mathcal{D}_p}\|_{\Omega_m}^2 + \|\nabla_{\mathcal{D}_f} v_{\mathcal{D}_p}\|_{\Omega_f}^2 + \|\nabla_{\mathcal{D}_g} v_{\mathcal{D}_g}\|_{\Omega_g}^2 + \|[\![v_\mathcal{D}]\!]_{\mathcal{D},\Gamma}\|_\Gamma^2 + \|[\![v_\mathcal{D}]\!]_{\mathcal{D},\Sigma_\Gamma}\|_{\Sigma_\Gamma}^2, \tag{10}$$

which is assumed to define a norm on $X_\mathcal{D}^0$. We now define coercivity, consistency, and limit conformity properties for sequences of gradient discretizations $(\mathcal{D}^l)_{l\in\mathbb{N}}$.

Let $C_\mathcal{D} > 0$ be defined by

$$C_\mathcal{D} \coloneqq \max_{v_\mathcal{D} \in X_\mathcal{D}^0 \setminus \{0\}} \frac{\|\Pi_{\mathcal{D}_m} v_{\mathcal{D}_p}\|_{\Omega_m} + \|\Pi_{\mathcal{D}_f} v_{\mathcal{D}_p}\|_{\Omega_f} + \|\Pi_{\mathcal{D}_g} v_{\mathcal{D}_g}\|_{\Omega_g}}{\|v_\mathcal{D}\|_\mathcal{D}}. \tag{11}$$

Definition 3.1 (Coercivity)**.** *A sequence of gradient discretizations $(\mathcal{D}^l)_{l\in\mathbb{N}}$ is said to be coercive if there exists $C_P > 0$ such that $C_{\mathcal{D}^l} \le C_P$ for all $l \in \mathbb{N}$.*

We define $S_{\mathcal{D}} : V_0 \times X_{\mathcal{D}}^0 \to \mathbb{R}$ such that, for all $u = (u_p, u_g) \in V_0$ and $v_{\mathcal{D}} = (v_{\mathcal{D}_p}, v_{\mathcal{D}_g}) \in X_{\mathcal{D}}^0$,

$$\begin{aligned} S_{\mathcal{D}}(u, v_{\mathcal{D}}) \coloneqq & \|\nabla_{\mathcal{D}_m} v_{\mathcal{D}_p} - \nabla u_p\|_{\Omega_m} + \|\nabla_{\mathcal{D}_f} v_{\mathcal{D}_p} - \nabla_\tau \gamma_f u_p\|_{\Omega_f} + \|\nabla_{\mathcal{D}_g} v_{\mathcal{D}_g} - u_g'\|_{\Omega_g} \\ & + \|\Pi_{\mathcal{D}_m} v_{\mathcal{D}_p} - u_p\|_{\Omega_m} + \|\Pi_{\mathcal{D}_f} v_{\mathcal{D}_p} - \gamma_f u_p\|_{\Omega_f} + \|\Pi_{\mathcal{D}_g} v_{\mathcal{D}_g} - u_g\|_{\Omega_g} \\ & + \|[\![v_{\mathcal{D}}]\!]_{\mathcal{D},\Gamma} - [\![u]\!]_\Gamma\|_\Gamma + \|[\![v_{\mathcal{D}}]\!]_{\mathcal{D},\Sigma_\Gamma} - [\![u]\!]_{\Sigma_\Gamma}\|_{\Sigma_\Gamma}, \end{aligned} \tag{12}$$

and

$$\mathcal{S}_{\mathcal{D}}(u) \coloneqq \inf_{v_{\mathcal{D}} \in X_{\mathcal{D}}^0} S_{\mathcal{D}}(u, v_{\mathcal{D}}). \tag{13}$$

Definition 3.2 (Consistency)**.** *A sequence of gradient discretizations $(\mathcal{D}^l)_{l\in\mathbb{N}}$ is said to be consistent if for all $u \in V_0$ one has $\lim_{l\to+\infty} \mathcal{S}_{\mathcal{D}^l}(u) = 0$.*

Let us define $W_{\mathcal{D}} : W \times X_{\mathcal{D}}^0 \to \mathbb{R}$ such that, for all $\boldsymbol{w} = (\boldsymbol{w}_m, \boldsymbol{w}_f, w_g) \in W$ and $v_{\mathcal{D}} = (v_{\mathcal{D}_p}, v_{\mathcal{D}_g}) \in X_{\mathcal{D}}^0$,

$$\begin{aligned} W_{\mathcal{D}}(\boldsymbol{w}, v_{\mathcal{D}}) \coloneqq & \int_{\Omega_m} (\boldsymbol{w}_m \cdot \nabla_{\mathcal{D}_m} v_{\mathcal{D}_p} + \Pi_{\mathcal{D}_m} v_{\mathcal{D}_p}\ \mathrm{div}(\boldsymbol{w}_m)) \mathrm{d}\boldsymbol{x} \\ & + \int_{\Omega_f} (\boldsymbol{w}_f \cdot \nabla_{\mathcal{D}_f} v_{\mathcal{D}_p} + \Pi_{\mathcal{D}_f} v_{\mathcal{D}_p}\ r_f(\boldsymbol{w}_p)) \mathrm{d}\tau(\boldsymbol{x}) \\ & + \int_{\Omega_g} (w_g \nabla_{\mathcal{D}_g} v_{\mathcal{D}_g} + \Pi_{\mathcal{D}_g} v_{\mathcal{D}_g}\ r_g(\boldsymbol{w})) \mathrm{d}x \\ & - \int_\Gamma (\boldsymbol{w}_m \cdot \boldsymbol{n}_\Gamma) [\![v_{\mathcal{D}}]\!]_{\mathcal{D},\Gamma} \mathrm{d}\tau(\boldsymbol{x}) - \int_{\Sigma_\Gamma} (\boldsymbol{w}_f \cdot \boldsymbol{n}_{\Sigma_\Gamma}) [\![v_{\mathcal{D}}]\!]_{\mathcal{D},\Sigma_\Gamma} \mathrm{d}l(\boldsymbol{x}), \end{aligned} \tag{14}$$

and

$$\mathcal{W}_{\mathcal{D}}(\boldsymbol{w}) \coloneqq \sup_{v_{\mathcal{D}} \in X_{\mathcal{D}}^0 \setminus \{0\}} \frac{|W_{\mathcal{D}}(\boldsymbol{w}, v_{\mathcal{D}})|}{\|v_{\mathcal{D}}\|_{\mathcal{D}}}. \tag{15}$$

Definition 3.3 (Limit conformity)**.** *A sequence of gradient discretizations $(\mathcal{D}^l)_{l\in\mathbb{N}}$ is said to be limit conforming if for all $\boldsymbol{w} \in W$ one has $\lim_{l\to+\infty} \mathcal{W}_{\mathcal{D}^l}(\boldsymbol{w}) = 0$.*

3.2 Application to the model problem

The gradient discretization $\mathcal{D}$ of (9) reads: Find $u_{\mathcal{D}} = (u_{\mathcal{D}_p}, u_{\mathcal{D}_g}) \in X_{\mathcal{D}}^0$ such that

$$\begin{aligned} & \int_{\Omega_m} \boldsymbol{\Lambda}_m \nabla_{\mathcal{D}_m} u_{\mathcal{D}_p} \cdot \nabla_{\mathcal{D}_m} v_{\mathcal{D}_p} \mathrm{d}\boldsymbol{x} + \int_{\Omega_f} d_f \boldsymbol{\Lambda}_f \nabla_{\mathcal{D}_f} u_{\mathcal{D}_p} \cdot \nabla_{\mathcal{D}_f} v_{\mathcal{D}_p} \mathrm{d}\tau(\boldsymbol{x}) \\ & + \int_{\Omega_g} |\omega_g| \Lambda_g \nabla_{\mathcal{D}_g} u_{\mathcal{D}_g} \nabla_{\mathcal{D}_g} v_{\mathcal{D}_g} \mathrm{d}x + \int_\Gamma H_g [\![u_{\mathcal{D}}]\!]_{\mathcal{D},\Gamma} [\![v_{\mathcal{D}}]\!]_{\mathcal{D},\Gamma} \mathrm{d}\tau(\boldsymbol{x}) \\ & + \int_{\Sigma_\Gamma} d_f H_g [\![u_{\mathcal{D}}]\!]_{\mathcal{D},\Sigma_\Gamma} [\![v_{\mathcal{D}}]\!]_{\mathcal{D},\Sigma_\Gamma} \mathrm{d}l(\boldsymbol{x}) \\ & = \int_{\Omega_m} \mathrm{f}_m \Pi_{\mathcal{D}_m} v_{\mathcal{D}_p} \mathrm{d}\boldsymbol{x} + \int_{\Omega_f} d_f \mathrm{f}_f \Pi_{\mathcal{D}_f} v_{\mathcal{D}_p} \mathrm{d}\tau(\boldsymbol{x}) + \int_{\Omega_g} |\omega_g| \mathrm{f}_g \Pi_{\mathcal{D}_g} v_{\mathcal{D}_g} \mathrm{d}x, \end{aligned} \tag{16}$$

for all $v_{\mathcal{D}} = (v_{\mathcal{D}_p}, v_{\mathcal{D}_g}) \in X_{\mathcal{D}}^0$. , we get the following results ensuring the well posedness of (16) and providing a priori error estimates.

Theorem 3.1 (Well-posedness)**.** *Let*

$$\mathcal{D} = \left(X_{\mathcal{D}}^0, \nabla_{\mathcal{D}_m}, \nabla_{\mathcal{D}_f}, \nabla_{\mathcal{D}_g}, \Pi_{\mathcal{D}_m}, \Pi_{\mathcal{D}_f}, \Pi_{\mathcal{D}_g}, [\![\cdot]\!]_{\mathcal{D},\Gamma}, [\![\cdot]\!]_{\mathcal{D},\Sigma_\Gamma}\right)$$

be a gradient discretization of the model problem (9), then the discrete formulation (16) has a unique solution $u_{\mathcal{D}} \in X_{\mathcal{D}}^0$. Moreover, the solution $u_{\mathcal{D}} \in X_{\mathcal{D}}^0$ satisfies the a priori estimate

$$\|u_{\mathcal{D}}\|_{\mathcal{D}} \leq \frac{C_{\mathcal{D}}}{\min(\underline{\lambda}_m, \underline{\lambda}_f \underline{d}_f, |\omega_g| \underline{\lambda}_g, \underline{H}_g, \underline{d}_f \underline{H}_g)} \left(\|\mathrm{f}_m\|_{\Omega_m} + \|d_f \mathrm{f}_f\|_{\Omega_f} + \||\omega_g| \mathrm{f}_g\|_{\Omega_g}\right).$$

Proof. For any solution $u_{\mathcal{D}} \in X_{\mathcal{D}}^0$ of (16), setting $v_{\mathcal{D}} = u_{\mathcal{D}}$ in (16), and using the Cauchy Schwarz inequality, the definition (11) of $C_{\mathcal{D}}$, and the assumption that $\|.\|_{\mathcal{D}}$ defines a norm on $X_{\mathcal{D}}^0$, we obtain the a priori estimate and hence the existence and uniqueness of a solution. □

Theorem 3.2 (Error estimates)**.** *Let $u = (u_p, u_g) \in V_0$ be the solution of (9) and let us set $\boldsymbol{q} = (\boldsymbol{q}_p, q_g) = (-\boldsymbol{\Lambda}_m \nabla u_p, -d_f \boldsymbol{\Lambda}_f \nabla_\tau \gamma_f u_p, -|\omega_g| \Lambda_g u_g') \in W$. Let $\mathcal{D}$ be a gradient discretization of (9), and let $u_{\mathcal{D}} \in X_{\mathcal{D}}^0$ be the solution of (16). Then, there exist two positive constants $C_1, C_2 > 0$ depending only on the physical parameters such that*

$$\begin{aligned} &\|\nabla_{\mathcal{D}_m} u_{\mathcal{D}_p} - \nabla u_p\|_{\Omega_m} + \|\nabla_{\mathcal{D}_f} u_{\mathcal{D}_p} - \nabla_\tau \gamma_f u_p\|_{\Omega_f} + \|\nabla_{\mathcal{D}_g} u_{\mathcal{D}_g} - u_g'\|_{\Omega_g} \\ &+ \|[\![u_{\mathcal{D}}]\!]_{\mathcal{D},\Gamma} - [\![u]\!]_\Gamma\|_\Gamma + \|[\![u_{\mathcal{D}}]\!]_{\mathcal{D},\Sigma_\Gamma} - [\![u]\!]_{\Sigma_\Gamma}\|_{\Sigma_\Gamma} \leq C_1 \mathcal{S}_{\mathcal{D}}(u) + C_2 \mathcal{W}_{\mathcal{D}}(\boldsymbol{q}). \end{aligned} \tag{17}$$

Moreover, there exist two positive constants $C_3, C_4 > 0$ depending only on $C_{\mathcal{D}}$ and the physical parameters such that

$$\begin{aligned} \|\Pi_{\mathcal{D}_m} u_{\mathcal{D}_p} - u_p\|_{\Omega_m} + \|\Pi_{\mathcal{D}_f} u_{\mathcal{D}_p} - \gamma_f u_p\|_{\Omega_f} + \|\Pi_{\mathcal{D}_g} u_{\mathcal{D}_g} - u_g\|_{\Omega_g} \\ \leq C_3 \mathcal{S}_{\mathcal{D}}(u) + C_4 \mathcal{W}_{\mathcal{D}}(\boldsymbol{q}). \end{aligned} \tag{18}$$

Proof. The two results (17) and (18) are obtained using the same arguments as in [17, Section 1.2], therefore the proof is omitted for sake of brevity. □

4 VAG discretization

We extend here the VAG discretization of [23] for diffusion problem adapted to general meshes and heterogenous anisotropic media to our model problem (9).

4.1 Mesh

4.1.1 The porous medium

The VAG method is built upon a polyhedral mesh of the domain Ω_p defined by prescribing a set of mesh elements $\mathcal{M}$, a set of mesh faces $\mathcal{F}$, a set of mesh edges $\mathcal{E}$ and a set of mesh vertex indices $\mathcal{V}$; we refer to [7, Definition 1] for a rigorous definition of those sets. For all $\kappa \in \mathcal{M}$, we denote by $\mathcal{F}_\kappa$, $\mathcal{E}_\kappa$ and $\mathcal{V}_\kappa$ the set of faces, edges and vertex indices of the cell κ, respectively. For all $\sigma \in \mathcal{F}$, we denote by $\mathcal{M}_\sigma$ the set of cells sharing the face σ, and by $\mathcal{E}_\sigma$ and $\mathcal{V}_\sigma$ the set of edges and vertex indices of the face σ, respectively. For all $e \in \mathcal{E}$, we denote by $\mathcal{M}_e$ and $\mathcal{F}_e$, the set of cells and faces, respectively, sharing the edge e, and by $\mathcal{V}_e$ the set of vertex indices of e. For all $\boldsymbol{s} \in \mathcal{V}$, we denote by $\mathcal{M}_{\boldsymbol{s}}$, $\mathcal{F}_{\boldsymbol{s}}$ and $\mathcal{E}_{\boldsymbol{s}}$ the set of cells, faces and edges sharing the vertex $\boldsymbol{x}_{\boldsymbol{s}}$, respectively. Let h_κ (respectively h_σ) denot the diameter of the mesh element $\kappa \in \mathcal{M}$ (respectively mesh face $\sigma \in \mathcal{F}$). The porous medium meshsize is defined by $h_{\mathcal{M}} = \max_{\kappa \in \mathcal{M}} h_\kappa$.

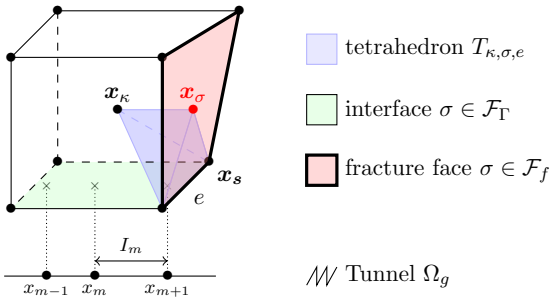

Figure 2: Illustration of notations introduced in Section 4.1.

Assumption 4.1 (Mesh regularity)**.** *We assume that for all $\kappa \in \mathcal{M}$ and all $\sigma \in \mathcal{F}$, there exist the so-called centers of κ and σ, respectively denoted by $\boldsymbol{x}_\kappa \in \kappa$ and $\boldsymbol{x}_\sigma \in \sigma$, so that both κ and σ are star-shaped with respect to their respective center.*

Assumption 4.1 implies that the porous medium mesh admits a particular matching tetrahedral submesh $\mathcal{T} = \{T_{\kappa,\sigma,e}\}_{\kappa\in\mathcal{M},\sigma\in\mathcal{F}_\kappa,e\in\mathcal{E}_\sigma}$, where for any $\kappa \in \mathcal{M}$, $\sigma \in \mathcal{F}_\kappa$ and $e \in \mathcal{E}_\kappa$, the tetrahedron $T_{\kappa,\sigma,e} \in \mathcal{T}$ is defined by the cell center $\boldsymbol{x}_\kappa$ and the triangular base $T_{\sigma,e} \subset \sigma$, which in turn is defined by the face center $\boldsymbol{x}_\sigma$ and the vertices $(\boldsymbol{x}_{\boldsymbol{s}})_{\boldsymbol{s}\in\mathcal{V}_e}$; see Figure 2. The families of tetrahedral submeshes will be assumed in the following to be shape regular in the sense that the shape regularity parameter defined by

$$\theta_{\mathcal{T}} = \max_{T\in\mathcal{T}} \frac{h_T}{\rho_T},$$

remains uniformly bounded, where h_T is the diameter and ρ_T is the insphere diameter of T. Together with Assumption 4.1, the shape regularity of the mesh sequence also implies that the maximum number of vertices of any mesh element remains bounded.

Assumption 4.2 (Geometric compliance)**.** *The porous medium mesh is assumed to be conforming with respect to the fracture network Ω_f, to the Dirichlet boundary Γ_D, and to the interface Γ, i.e. there exist subsets $\mathcal{F}_f, \mathcal{F}_\Gamma, \mathcal{F}_D \subset \mathcal{F}$ and $\mathcal{E}_{\Sigma_\Gamma}, \mathcal{E}_{\Sigma_D}, \mathcal{E}_{\Sigma_N} \subset \mathcal{E}$ such that*

$$\overline{\Omega_f} = \bigcup_{\sigma\in\mathcal{F}_f} \overline{\sigma},\ \overline{\Gamma} = \bigcup_{\sigma\in\mathcal{F}_\Gamma} \overline{\sigma},\ \overline{\Gamma_D} = \bigcup_{\sigma\in\mathcal{F}_D} \overline{\sigma},\ \overline{\Sigma_\Gamma} = \bigcup_{e\in\mathcal{E}_{\Sigma_\Gamma}} \overline{e},\ \overline{\Sigma_D} = \bigcup_{e\in\mathcal{E}_{\Sigma_D}} \overline{e},\ \overline{\Sigma_N} = \bigcup_{e\in\mathcal{E}_{\Sigma_N}} \overline{e}.$$

We also define the following subsets of vertex indices:

$$\mathcal{V}_f = \bigcup_{\sigma\in\mathcal{F}_f} \mathcal{V}_\sigma,\quad \mathcal{V}_\Gamma = \bigcup_{\sigma\in\mathcal{F}_\Gamma} \mathcal{V}_\sigma,\quad \mathcal{V}_{\Sigma_\Gamma} = \bigcup_{e\in\mathcal{E}_\Gamma} \mathcal{V}_e,\quad \mathcal{V}_D = \bigcup_{\sigma\in\mathcal{F}_D} \mathcal{V}_\sigma \setminus \mathcal{V}_\Gamma.$$

Note that $\mathcal{V}_D$ and $\mathcal{V}_\Gamma$ must be such that $\mathcal{V}_D \cap \mathcal{V}_\Gamma = \emptyset$ and that our choice above assumes $\mathcal{V}_D \cap \overline{\Gamma} = \emptyset$ to fix ideas.

According to the context and with a slight abuse of notation, we will denote by $|X|$ either (i) the Lebesgue d_X-dimensional measure of X when $X \subset \overline{\Omega_p}$ of dimension d_X, or (ii) the cardinal of X when X is a finite collection of objects.

4.1.2 The tunnel

On the tunnel side, the finite element method is built upon a nonconforming (with respect to the interface nodes) one-dimensional mesh of Ω_g defined prescribing a set of tunnel mesh

elements $\mathcal{G}$ and a set of tunnel vertex indices $\mathcal{V}_\mathcal{G}$. The set of tunnel mesh elements

$$\mathcal{G} = \{I_m = (x_m, x_{m+1})\}_{m\in\{0,\cdots,m_L\}},$$

denotes the finite collection of open disjoint line segments given by (m_L+2) vertices in $\overline{\Omega_g}$ such that $x_0 = 0$, $x_{m_L+1} = L$ and $x_m < x_{m+1}$ for all $m \in \{0,\cdots,m_L\}$. The set of tunnel vertex indices $\mathcal{V}_\mathcal{G} = \{0,\cdots,m_L+1\}$ is a finite collection of indices m associated with vertices x_m. The dual mesh of $\mathcal{G}$ is denoted by

$$\mathcal{G}^\star = \{I_m^\star = (x_{m-1/2}, x_{m+1/2})\}_{m\in\{1,\cdots,m_L\}},$$

and defined by the finite collection of open disjoint line segments given by m_L+1 vertices in $\overline{\Omega_g}$ such that $x_{1/2} = 0$, $x_{m_L+1/2} = L$ and $x_{m+1/2} = {}^{(x_m+x_{m+1})}/_2$ for all $m \in \{1,\cdots,m_L-1\}$. Finally, we set $h_m = |x_{m+1} - x_m|$ for all $m \in \{0,\cdots,m_L\}$ and $h_\mathcal{G} = \max_{m\in\{0,\cdots,m_L\}} h_m$.

Remark 4.1 (Nonconforming meshes at the interface Γ)**.** *We stress that we do not assume here the geometric compliance at the interface Γ between the porous medium and the tunnel, which would require that $\{x_{\boldsymbol{s}} \mid \boldsymbol{s} \in \mathcal{V}_\Gamma\} = \{x_m \mid m \in \mathcal{V}_\mathcal{G}\}$. That way, the meshing procedure of the porous medium and the tunnel can be carried out completely independently.*

4.2 Discrete settings

In this section, we define the degrees of freedom (DOFs), mapping and direcrete reconstruction operators underlying the VAG method.

4.2.1 Degrees of freedom and mapping operators

We define the vector spaces of the porous medium and tunnel DOFs as

$$X_{\mathcal{D}_p} \coloneqq \left\{\left((v_\kappa)_{\kappa\in\mathcal{M}}, (v_{\boldsymbol{s}})_{\boldsymbol{s}\in\mathcal{V}}, (v_\sigma)_{\sigma\in\mathcal{F}_f}\right) \in \mathbb{R}^{|\mathcal{M}|+|\mathcal{V}|+|\mathcal{F}_f|}\right\}, \quad X_{\mathcal{D}_g} \coloneqq \{(v_m)_{m\in\mathcal{V}_\mathcal{G}} \in \mathbb{R}^{|\mathcal{V}_\mathcal{G}|}\}. \tag{19}$$

Those DOFs are localized at the cell centers $(\boldsymbol{x}_\kappa)_{\kappa\in\mathcal{M}}$, fracture face centers $(\boldsymbol{x}_\sigma)_{\sigma\in\mathcal{F}_f}$ and nodes $(\boldsymbol{x}_{\boldsymbol{s}})_{\boldsymbol{s}\in\mathcal{V}}$ of the porous medium mesh, and at the tunnel vertices $(x_m)_{m\in\mathcal{V}_\mathcal{G}}$. The global vector space of DOFs is denoted by $X_\mathcal{D}$ and is defined by the cartesian product of the vector spaces

$$X_\mathcal{D} \coloneqq X_{\mathcal{D}_p} \times X_{\mathcal{D}_g}. \tag{20}$$

We also define the vector subspace of $X_\mathcal{D}$ with strongly enforced homogeneous Dirichlet boundary conditions on Γ_D, Σ_D and on the tunnel boundary nodes $x \in \{0, L\}$

$$X_\mathcal{D}^0 \coloneqq \{v_\mathcal{D} \in X_\mathcal{D} \,|\, v_{\boldsymbol{s}} = 0 \text{ for all } \boldsymbol{s} \in \mathcal{V}_D, \text{ and } v_0 = v_{m_L+1} = 0\}. \tag{21}$$

Then, we define the interpolation operators $\mathcal{P}_{\mathcal{D}_p} : \mathcal{C}^0(\overline{\Omega_p}) \to X_{\mathcal{D}_p}$ and $\mathcal{P}_{\mathcal{D}_g} : \mathcal{C}^0(\overline{\Omega_g}) \to X_{\mathcal{D}_g}$ such that, for all $\varphi_p \in \mathcal{C}^0(\overline{\Omega_p})$ and all $\varphi_g \in \mathcal{C}^0(\overline{\Omega_g})$,

$$\begin{aligned}
\mathcal{P}_{\mathcal{D}_p}\varphi_p &= \left((\varphi_p(\boldsymbol{x}_\kappa))_{\kappa\in\mathcal{M}}, (\varphi_p(\boldsymbol{x}_{\boldsymbol{s}}))_{\boldsymbol{s}\in\mathcal{V}}, (\varphi_p(\boldsymbol{x}_\sigma))_{\sigma\in\mathcal{F}_f}\right)\\
\mathcal{P}_{\mathcal{D}_g}\varphi_g &= \left((\varphi_g(x_m))_{m\in\mathcal{V}_\mathcal{G}}\right)
\end{aligned} \tag{22}$$

and we denote by $\mathcal{P}_\mathcal{D} : \mathcal{C}^0(\overline{\Omega_p}) \times \mathcal{C}^0(\overline{\Omega_g}) \to X_\mathcal{D}$ the global operator defined such that $\mathcal{P}_\mathcal{D}\varphi = (\mathcal{P}_{\mathcal{D}_p}\varphi_p, \mathcal{P}_{\mathcal{D}_g}\varphi_g)$ for any $\varphi = (\varphi_p, \varphi_g) \in \mathcal{C}^0(\overline{\Omega_p}) \times \mathcal{C}^0(\overline{\Omega_g})$.

4.2.2 Discrete reconstruction operators

In this section we introduce the reconstruction operators underlying the VAG discretization. The key ingredient lies in the definition of the discrete jump operators which must account for the mesh nonconformity at the porous medium-tunnel interface. They are chosen such that (i) they lead to local expressions of the interface fluxes, (ii) they are readily extended to more complex geometries using the surjective mapping from Γ to Ω_g, (iii) the limit scheme obtained for $H_g \to +\infty$ provides a first order accurate discretization of the limit model (see Remark 2.1).

Function reconstruction operators. First, we define the following partition of each cell $\kappa \in \mathcal{M}$ and each fracture face $\sigma \in \mathcal{F}_f$

$$\overline{\kappa} \;=\; \overline{\omega}_\kappa \bigcup \left(\bigcup_{\boldsymbol{s} \in \mathcal{V}_\kappa \setminus (\mathcal{V}_D \cup \mathcal{V}_\Gamma \cup \mathcal{V}_f)} \overline{\omega}_{\kappa,\boldsymbol{s}} \right), \quad \overline{\sigma} \;=\; \overline{\omega}_\sigma \bigcup \left(\bigcup_{\boldsymbol{s} \in \mathcal{V}_\sigma \setminus (\mathcal{V}_D \cup \mathcal{V}_\Gamma)} \overline{\omega}_{\sigma,\boldsymbol{s}} \right).$$

The piecewise constant function reconstruction operators are defined in the matrix $\Pi_{\mathcal{D}_m} : X_{\mathcal{D}_p} \to L^2(\Omega_p)$, in the fracture network $\Pi_{\mathcal{D}_f} : X_{\mathcal{D}_p} \to L^2(\Omega_f)$ and in the tunnel $\Pi_{\mathcal{D}_g} : X_{\mathcal{D}_g} \to L^2(\Omega_g)$, and are such that

$$\forall v_{\mathcal{D}_p} \in X_{\mathcal{D}_p}, \quad \Pi_{\mathcal{D}_m} v_{\mathcal{D}_p}(\boldsymbol{x}) = \begin{cases} v_\kappa & \text{for all } \boldsymbol{x} \in \omega_\kappa,\ \kappa \in \mathcal{M}, \\ v_{\boldsymbol{s}} & \text{for all } \boldsymbol{x} \in \omega_{\kappa,\boldsymbol{s}},\ \kappa \in \mathcal{M},\ \boldsymbol{s} \in \mathcal{V}_\kappa \setminus (\mathcal{V}_D \cup \mathcal{V}_\Gamma \cup \mathcal{V}_f), \end{cases} \tag{23a}$$

$$\Pi_{\mathcal{D}_f} v_{\mathcal{D}_p}(\boldsymbol{x}) = \begin{cases} v_\sigma & \text{for all } \boldsymbol{x} \in \omega_\sigma,\ \sigma \in \mathcal{F}_f, \\ v_{\boldsymbol{s}} & \text{for all } \boldsymbol{x} \in \omega_{\sigma,\boldsymbol{s}},\ \sigma \in \mathcal{F}_f,\ \boldsymbol{s} \in \mathcal{V}_\sigma \setminus (\mathcal{V}_D \cup \mathcal{V}_{\Sigma_\Gamma}), \end{cases} \tag{23b}$$

$$\forall v_{\mathcal{D}_g} \in X_{\mathcal{D}_g}, \quad \Pi_{\mathcal{D}_g} v_{\mathcal{D}_g}(x) = v_m \text{ for all } x \in I_m^\star,\ I_m^\star \in \mathcal{G}^\star. \tag{23c}$$

Note that $\Pi_{\mathcal{D}_m} v_{\mathcal{D}_p}$ does not depend on $v_{\boldsymbol{s}}$ for all $\boldsymbol{s} \in \mathcal{V}_f \cup \mathcal{V}_\Gamma$ and that $\Pi_{\mathcal{D}_m} v_{\mathcal{D}_f}$ does not depend on $v_{\boldsymbol{s}}$ for all $\boldsymbol{s} \in \mathcal{V}_{\Sigma_\Gamma}$. This choice avoids the mixing of matrix and fracture quantities in the control volumes located at nodes $\boldsymbol{x}_{\boldsymbol{s}}$ for all $\boldsymbol{s} \in \mathcal{V}_f$, as well as the mixing of porous medium and tunnel quantities in the control volumes located at nodes $\boldsymbol{x}_{\boldsymbol{s}}$ for all $\boldsymbol{s} \in \mathcal{V}_\Gamma$. This a crutial property for the extension of the scheme to transport models such as the one presented in Section 5.2.

Gradient reconstruction operators. We then define the global spaces of continuous piecewise affine functions on the tetrahedral submesh $\mathcal{T}$ as $\mathbb{P}_1(\mathcal{T}) \coloneqq \left\{ v \in \mathcal{C}^0(\overline{\Omega_p}) \mid v_{|T} \in \mathbb{P}_1(T)\ \forall T \in \mathcal{T} \right\}$ and on the tunnel mesh $\mathcal{G}$ as $\mathbb{P}_1(\mathcal{G}) \coloneqq \left\{ w \in \mathcal{C}^0(\overline{\Omega}_g) \mid w_{|I_m} \in \mathbb{P}_1(I_m)\ \forall I_m \in \mathcal{G} \right\}$. The continuous piecewise affine function reconstruction operators in the porous medium and in the tunnel, respectively denoted by $\Pi_{\mathcal{T}} : X_{\mathcal{D}_p} \to \mathbb{P}_1(\mathcal{T})$ and $\Pi_{\mathcal{G}} : X_{\mathcal{D}_g} \to \mathbb{P}_1(\mathcal{G})$, are defined such that

$$\begin{aligned} \forall v_{\mathcal{D}_p} \in X_{\mathcal{D}_p}, \quad & \Pi_{\mathcal{T}} v_{\mathcal{D}_p}(\boldsymbol{x}_\kappa) = v_\kappa \text{ for all } \kappa \in \mathcal{M}, \\ & \Pi_{\mathcal{T}} v_{\mathcal{D}_p}(\boldsymbol{x}_{\boldsymbol{s}}) = v_{\boldsymbol{s}} \text{ for all } \boldsymbol{s} \in \mathcal{V}, \\ & \Pi_{\mathcal{T}} v_{\mathcal{D}_p}(\boldsymbol{x}_\sigma) = \begin{cases} v_\sigma & \text{for all } \sigma \in \mathcal{F}_f \\ |\mathcal{V}_\sigma|^{-1} \sum_{\boldsymbol{s} \in \mathcal{V}_\sigma} v_{\boldsymbol{s}} & \text{for all } \sigma \in \mathcal{F} \setminus \mathcal{F}_f \end{cases}, \\ \forall v_{\mathcal{D}_g} \in X_{\mathcal{D}_g}, \quad & \Pi_{\mathcal{G}} v_{\mathcal{D}_g}(x) = \sum_{m \in \mathcal{V}_{\mathcal{G}}} \eta_m^g(x) v_m \text{ for all } x \in \overline{\Omega_g}, \end{aligned} \tag{24}$$

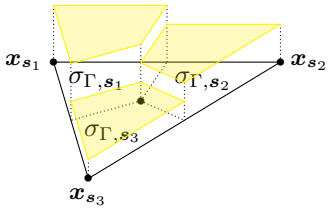

Figure 3: Example of lumped basis function supports for a face $\sigma \in \mathcal{F}_\Gamma$. The supports are such that $|\sigma_{\Gamma,\boldsymbol{s}_i} \cap \sigma| = \int_\sigma \eta^p_{\boldsymbol{s}_i}(\boldsymbol{x})\mathrm{d}\tau(\boldsymbol{x})$ for $i \in \{1,2,3\}$, where $\eta^p_{\boldsymbol{s}_i}$ is the nodal basis function of $\Pi_\mathcal{T} X_{\mathcal{D}_p}$ associated to $\boldsymbol{s}_i$.

where, $\eta^g_m(\cdot)$, $m \in \mathcal{V}_\mathcal{G}$ denotes the nodal finite element basis of the finite element space $\mathbb{P}_1(\mathcal{G})$. We then define the gradient reconstruction operators in the matrix $\nabla_{\mathcal{D}_m} : X_{\mathcal{D}_p} \to L^2(\Omega_p)^3$, in the fracture network $\nabla_{\mathcal{D}_f} : X_{\mathcal{D}_p} \to L^2(\Omega_f)^2$ and in the tunnel $\nabla_{\mathcal{D}_g} : X_{\mathcal{D}_g} \to L^2(\Omega_g)$ such that

$$\forall v_{\mathcal{D}_p} \in X_{\mathcal{D}_p}, \quad \nabla_{\mathcal{D}_m} v_{\mathcal{D}_p} \coloneqq \nabla \Pi_\mathcal{T} v_{\mathcal{D}_p}, \tag{25a}$$

$$\nabla_{\mathcal{D}_f} v_{\mathcal{D}_p} \coloneqq \nabla_\tau \gamma_f \Pi_\mathcal{T} v_{\mathcal{D}_p}, \tag{25b}$$

$$\forall v_{\mathcal{D}_g} \in X_{\mathcal{D}_g}, \quad \nabla_{\mathcal{D}_g} v_{\mathcal{D}_g}(x) \coloneqq (\Pi_\mathcal{G} v_{\mathcal{D}_g})'. \tag{25c}$$

Jump reconstruction operators. Finally, we introduce the discrete counterparts of the jump operators $[\![\cdot]\!]_\Gamma$ and $[\![\cdot]\!]_{\Sigma_\Gamma}$. In the spirit of [8, Section 4.1] and in order to obtain a local expression of the interface fluxes, the traces of the finite element basis functions are lumped in order to define jump operators as piecewise constant function reconstructions on dual meshes of $\mathcal{F}_\Gamma$ and $\mathcal{E}_{\Sigma_\Gamma}$. Let us denote by $(\sigma_{\Gamma,\boldsymbol{s}})_{\boldsymbol{s}\in\mathcal{V}_\Gamma}$ and $(e_{\Sigma_\Gamma,\boldsymbol{s}})_{\boldsymbol{s}\in\mathcal{V}_{\Sigma_\Gamma}}$ the supports of the lumped basis functions; see, e.g. Figure 3.

Note that the lumping of the basis functions is such that, for any $v_{\mathcal{D}_p} \in X_{\mathcal{D}_p}$

$$\int_\sigma \left(\gamma_\Gamma \Pi_\mathcal{T} v_{\mathcal{D}_p} - \sum_{\boldsymbol{s}\in\mathcal{V}_\Gamma} v_{\boldsymbol{s}} \mathbf{1}_{\sigma_{\Gamma,\boldsymbol{s}}} \right) \mathrm{d}\tau(\boldsymbol{x}) = 0 \qquad \forall \sigma \in \mathcal{F}_\Gamma, \tag{26a}$$

$$\int_e \left(\gamma_{\Sigma_\Gamma} \gamma_f \Pi_\mathcal{T} v_{\mathcal{D}_p} - \sum_{\boldsymbol{s}\in\mathcal{V}_{\Sigma_\Gamma}} v_{\boldsymbol{s}} \mathbf{1}_{e_{\Sigma_\Gamma,\boldsymbol{s}}} \right) \mathrm{d}l(\boldsymbol{x}) = 0 \qquad \forall e \in \mathcal{E}_{\Sigma_\Gamma}, \tag{26b}$$

where $\mathbf{1}_X$ denotes the characteristic function defined on X. Then, the jump operators are defined by

$$[\![v_\mathcal{D}]\!]_{\mathcal{D},\Gamma} = \sum_{\boldsymbol{s}\in\mathcal{V}_\Gamma} (v_{\boldsymbol{s}} - \Pi_\mathcal{G} v_{\mathcal{D}_g}(x_{\boldsymbol{s}})) \mathbf{1}_{\sigma_{\Gamma,\boldsymbol{s}}}, \qquad [\![v_\mathcal{D}]\!]_{\mathcal{D},\Sigma_\Gamma} = \sum_{\boldsymbol{s}\in\mathcal{V}_{\Sigma_\Gamma}} (v_{\boldsymbol{s}} - \Pi_\mathcal{G} v_{\mathcal{D}_g}(x_{\boldsymbol{s}})) \mathbf{1}_{e_{\Sigma_\Gamma,\boldsymbol{s}}}, \tag{27}$$

For all $m \in \mathcal{V}_\mathcal{G}$ and all $\boldsymbol{s} \in \mathcal{V}_\Gamma$, we wil use the notation $\eta^g_{m,\boldsymbol{s}} \coloneqq \eta^g_m(x_{\boldsymbol{s}})$ for the evaluation of the tunnel basis function $\eta^g_m(\cdot)$ at the x-coordinate of the node $\boldsymbol{x}_{\boldsymbol{s}} = (x_{\boldsymbol{s}}, y_{\boldsymbol{s}}, z_{\boldsymbol{s}})$.

4.3 Discrete variational and finite volume formulations

In this section, we derive the equivalent finite volume formulation of the VAG discretization (16). It will be used for the extension of the discretization to the drying model presented in Subsection 5.2.

4.3.1 Discrete variational formulation

The discrete variational formulation of the model problem (9) is directly given by (16) using the vector space of DOFs (21), the function reconstruction operators (23), the discrete gradient reconstruction operators (25) and the jump reconstruction operators (27).

4.3.2 Finite volume formulation

In order to write the equivalent finite volume formulation of (16), let us define for all $u_{\mathcal{D}_p} \in X_{\mathcal{D}_p}$ the matrix fluxes

$$V_{\kappa,\nu}(u_{\mathcal{D}_p}) = \sum_{\nu' \in \Xi_\kappa} T_\kappa^{\nu,\nu'}(u_\kappa - u_{\nu'}), \text{ with } T_\kappa^{\nu,\nu'} = \int_\kappa \mathbf{\Lambda}_m \nabla \eta_\nu^p \cdot \nabla \eta_{\nu'}^p \mathrm{d}\boldsymbol{x}. \tag{28}$$

connecting each cell $\kappa \in \mathcal{M}$ to its DOFs $\nu \in \Xi_\kappa := \mathcal{V}_\kappa \cup (\mathcal{F}_\kappa \cap \mathcal{F}_f)$. The transmissivities $T_\kappa^{\nu,\nu'}$ are defined above using the nodal finite element basis of $\Pi_\mathcal{T} X_{\mathcal{D}_p}$ denoted by η_ν^p, $\nu \in \mathcal{M} \cup \mathcal{V} \cup \mathcal{F}_f$. Similarly, the fracture fluxes defined by

$$V_{\sigma,\boldsymbol{s}}(u_{\mathcal{D}_p}) = \sum_{\boldsymbol{s}' \in \mathcal{V}_\sigma} T_\sigma^{\boldsymbol{s},\boldsymbol{s}'}(u_\sigma - u_{\boldsymbol{s}'}), \text{ with } T_\sigma^{\boldsymbol{s},\boldsymbol{s}'} = \int_\sigma d_f \mathbf{\Lambda}_f \nabla_\tau \gamma_f \eta_{\boldsymbol{s}}^p \cdot \nabla_\tau \gamma_f \eta_{\boldsymbol{s}'}^p \mathrm{d}\tau(\boldsymbol{x}), \tag{29}$$

connect each fracture face $\sigma \in \mathcal{F}_f$ to its nodes $\boldsymbol{x}_{\boldsymbol{s}}$ with $\boldsymbol{s} \in \mathcal{V}_\sigma$. On the tunnel side, we similarly define for all $u_{\mathcal{D}_g} \in X_{\mathcal{D}_g}$ the fluxes

$$V_{m,m+1}(u_{\mathcal{D}_g}) = T_{m+\frac{1}{2}}(u_m - u_{m+1}), \text{ with } T_{m+\frac{1}{2}} = \frac{|\omega_g|}{h_m^2} \int_{x_m}^{x_{m+1}} \Lambda_g(x)\mathrm{d}x, \tag{30}$$

connecting the node x_m to x_{m+1} for all $m \in \{0, \cdots, m_L\}$. Setting

$$T_{\Gamma,\boldsymbol{s}} = \int_{\sigma_{\Gamma,\boldsymbol{s}}} H_g(\boldsymbol{x})\mathrm{d}\tau(\boldsymbol{x}), \qquad T_{\Sigma_\Gamma,\boldsymbol{s}} = \int_{e_{\Sigma_\Gamma,\boldsymbol{s}}} d_f(\boldsymbol{x}) H_g(\boldsymbol{x})\mathrm{d}l(\boldsymbol{x}),$$

we obtain, for all $\boldsymbol{s} \in \mathcal{V}_\Gamma$ and all $m \in \mathcal{V}_\mathcal{G}$, the fluxes

$$V_{\boldsymbol{s},m}^\Gamma(u_\mathcal{D}) = \sum_{m' \in \mathcal{V}_\mathcal{G}} \eta_{m,\boldsymbol{s}}^g \eta_{m',\boldsymbol{s}}^g T_{\Gamma,\boldsymbol{s}}(u_{\boldsymbol{s}} - u_{m'}) = \eta_{m,\boldsymbol{s}}^g T_{\Gamma,\boldsymbol{s}} \left(u_{\boldsymbol{s}} - \sum_{m' \in \mathcal{V}_\mathcal{G}} \eta_{m',\boldsymbol{s}}^g u_{m'} \right),$$

and, for all $\boldsymbol{s} \in \mathcal{V}_{\Sigma_\Gamma}$ and all $m \in \mathcal{V}_\mathcal{G}$, the fluxes

$$V_{\boldsymbol{s},m}^{\Sigma_\Gamma}(u_\mathcal{D}) = \sum_{m' \in \mathcal{V}_\mathcal{G}} \eta_{m,\boldsymbol{s}}^g \eta_{m',\boldsymbol{s}}^g T_{\Sigma_\Gamma,\boldsymbol{s}}(u_{\boldsymbol{s}} - u_{m'}) = \eta_{m,\boldsymbol{s}}^g T_{\Sigma_\Gamma,\boldsymbol{s}}(u_{\boldsymbol{s}} - \sum_{m' \in \mathcal{V}_\mathcal{G}} \eta_{m',\boldsymbol{s}}^g u_{m'}).$$

Figure 4 illustrates the configuration of these fluxes in the case of a given cell κ with one fracture face σ.

Let us set for the source terms in the matrix

$$\mathrm{f}_{m,\kappa} = \frac{1}{|\omega_\kappa|} \int_{\omega_\kappa} \mathrm{f}_m(\boldsymbol{x})\mathrm{d}\boldsymbol{x}, \qquad \mathrm{f}_{m,\kappa,\boldsymbol{s}} = \frac{1}{|\omega_{\kappa,\boldsymbol{s}}|} \int_{\omega_{\kappa,\boldsymbol{s}}} \mathrm{f}_m(\boldsymbol{x})\mathrm{d}\boldsymbol{x},$$

and $\alpha_{\kappa,\boldsymbol{s}} = \frac{|\omega_{\kappa,\boldsymbol{s}}|}{|\kappa|}$ for all $\kappa \in \mathcal{M}$ and all $\boldsymbol{s} \in \mathcal{V}_\kappa \setminus (\mathcal{V}_D \cup \mathcal{V}_\Gamma \cup \mathcal{V}_f)$. Similarly, we set in the fracture network

$$\mathrm{f}_{f,\sigma} = \frac{1}{|\omega_\sigma|} \int_{\omega_\sigma} d_f(\boldsymbol{x}) \mathrm{f}_f(\boldsymbol{x})\mathrm{d}\tau(\boldsymbol{x}), \qquad \mathrm{f}_{f,\sigma,\boldsymbol{s}} = \frac{1}{|\omega_{\sigma,\boldsymbol{s}}|} \int_{\omega_{\sigma,\boldsymbol{s}}} d_f(\boldsymbol{x}) \mathrm{f}_f(\boldsymbol{x})\mathrm{d}\tau(\boldsymbol{x}),$$

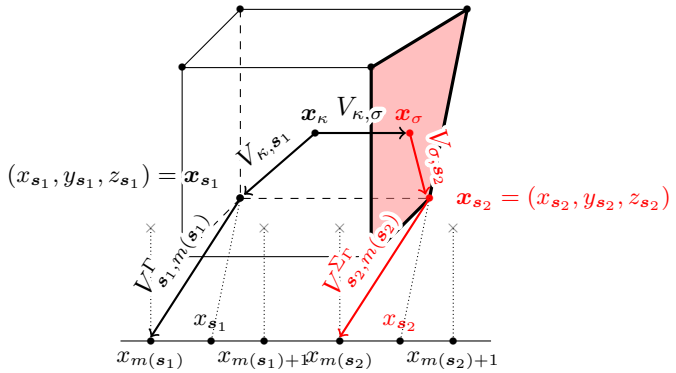

Figure 4: Geometric representation of the fluxes defined in Section 4.3.2. The index $m(\boldsymbol{s})$ is such that $x_{\boldsymbol{s}} \in [x_{m(\boldsymbol{s})}, x_{m(\boldsymbol{s})+1})$. The interface fluxes are defined by $V^{\Gamma}_{\boldsymbol{s}_1,m(\boldsymbol{s}_1)} = \eta^g_{m(\boldsymbol{s}_1),\boldsymbol{s}_1} T_{\Gamma,\boldsymbol{s}_1} \left(u_{\boldsymbol{s}_1} - \eta^g_{m(\boldsymbol{s}_1),\boldsymbol{s}_1} u_{m(\boldsymbol{s}_1)} - \eta^g_{m(\boldsymbol{s}_1)+1,\boldsymbol{s}_1} u_{m(\boldsymbol{s}_1)+1}\right)$ and $V^{\Sigma_\Gamma}_{\boldsymbol{s}_2,m(\boldsymbol{s}_2)} = \eta^g_{m(\boldsymbol{s}_2),\boldsymbol{s}_2} T_{\Sigma_\Gamma,\boldsymbol{s}_2} \left(u_{\boldsymbol{s}_2} - \eta^g_{m(\boldsymbol{s}_2),\boldsymbol{s}_2} u_{m(\boldsymbol{s}_2)} - \eta^g_{m(\boldsymbol{s}_2)+1,\boldsymbol{s}_2} u_{m(\boldsymbol{s}_2)+1}\right)$.

and $\alpha_{\sigma,\boldsymbol{s}} = \frac{|\omega_{\sigma,\boldsymbol{s}}|}{|\sigma|}$ for all $\sigma \in \mathcal{F}_f$ and all $\boldsymbol{s} \in \mathcal{V}_\sigma \setminus (\mathcal{V}_D \cup \mathcal{V}_{\Sigma_\Gamma})$. Then, the discrete formulation (16) is equivalent to find $u_{\mathcal{D}} = (u_{\mathcal{D}_p}, u_{\mathcal{D}_g}) \in X^0_{\mathcal{D}}$ satisfying the discrete conservation equations in the porous medium

$$
\begin{cases}
\displaystyle\sum_{\nu\in\Xi_K} V_{\kappa,\nu}(u_{\mathcal{D}_p}) = (1 - \sum_{\boldsymbol{s}\in\mathcal{V}_K\setminus(\mathcal{V}_D\cup\mathcal{V}_\Gamma\cup\mathcal{V}_f)} \alpha_{\kappa,\boldsymbol{s}})|\kappa|\mathrm{f}_{m,\kappa}, & \forall \kappa \in \mathcal{M}, \\
\displaystyle\sum_{\boldsymbol{s}\in\mathcal{V}_\sigma} V_{\sigma,\boldsymbol{s}}(u_{\mathcal{D}_p}) - \sum_{\kappa\in\mathcal{M}_\sigma} V_{\kappa,\sigma}(u_{\mathcal{D}_p}) = (1 - \sum_{\boldsymbol{s}\in\mathcal{V}_\sigma\setminus(\mathcal{V}_D\cup\mathcal{V}_\Gamma)} \alpha_{\sigma,\boldsymbol{s}})|\sigma|\mathrm{f}_{f,\sigma}, & \forall \sigma \in \mathcal{F}_f, \\
\displaystyle\sum_{\kappa\in\mathcal{M}_{\boldsymbol{s}}} -V_{\kappa,\boldsymbol{s}}(u_{\mathcal{D}_p}) = \sum_{\kappa\in\mathcal{M}_{\boldsymbol{s}}} \alpha_{\kappa,\boldsymbol{s}}|\kappa|\mathrm{f}_{m,\kappa,\boldsymbol{s}}, & \forall \boldsymbol{s} \in \mathcal{V} \setminus (\mathcal{V}_D \cup \mathcal{V}_\Gamma \cup \mathcal{V}_f), \\
\displaystyle\sum_{\kappa\in\mathcal{M}_{\boldsymbol{s}}} -V_{\kappa,\boldsymbol{s}}(u_{\mathcal{D}_p}) + \sum_{\sigma\in\mathcal{F}_{f,\boldsymbol{s}}} -V_{\sigma,\boldsymbol{s}}(u_{\mathcal{D}_p}) = \sum_{\sigma\in\mathcal{F}_{f,\boldsymbol{s}}} \alpha_{\sigma,\boldsymbol{s}}|\sigma|\mathrm{f}_{f,\sigma,\boldsymbol{s}}, & \forall \boldsymbol{s} \in \mathcal{V}_f \setminus (\mathcal{V}_D \cup \mathcal{V}_{\Sigma_\Gamma}), \\
\displaystyle\sum_{\kappa\in\mathcal{M}_{\boldsymbol{s}}} -V_{\kappa,\boldsymbol{s}}(u_{\mathcal{D}_p}) + \sum_{m\in\mathcal{V}_{\mathcal{G}}} V^{\Gamma}_{\boldsymbol{s},m}(u_{\mathcal{D}}) = 0, & \forall \boldsymbol{s} \in \mathcal{V}_\Gamma \setminus \mathcal{V}_{\Sigma_\Gamma}, \\
\displaystyle\sum_{\kappa\in\mathcal{M}_{\boldsymbol{s}}} -V_{\kappa,\boldsymbol{s}}(u_{\mathcal{D}_p}) + \sum_{\sigma\in\mathcal{F}_{f,\boldsymbol{s}}} -V_{\sigma,\boldsymbol{s}}(u_{\mathcal{D}_p}) & \\
\qquad + \displaystyle\sum_{m\in\mathcal{V}_{\mathcal{G}}} V^{\Gamma}_{\boldsymbol{s},m}(u_{\mathcal{D}}) + \sum_{m\in\mathcal{V}_{\mathcal{G}}} V^{\Sigma_\Gamma}_{\boldsymbol{s},m}(u_{\mathcal{D}}) = 0, & \forall \boldsymbol{s} \in \mathcal{V}_{\Sigma_\Gamma},
\end{cases}
\tag{31}
$$

coupled with the conservation equations in the tunnel for all $m \in \{1, \cdots, m_L\}$

$$
V_{m,m+1}(u_{\mathcal{D}_g}) - V_{m-1,m}(u_{\mathcal{D}_g}) - \sum_{\boldsymbol{s}\in\mathcal{V}_\Gamma} V^{\Gamma}_{\boldsymbol{s},m}(u_{\mathcal{D}}) - \sum_{\boldsymbol{s}\in\mathcal{V}_{\Sigma_\Gamma}} V^{\Sigma_\Gamma}_{\boldsymbol{s},m}(u_{\mathcal{D}}) = \int_{x_{m-1/2}}^{x_{m+1/2}} |\omega_g|\mathrm{f}_g \mathrm{d}x. \tag{32}
$$

4.4 Main results

In this subsection we report the main results of the analysis of the VAG discretization, postponing the proofs to Section 7.2.

Proposition 4.1 (Gradient scheme)**.** *For any family of shape regular meshes, the VAG discretization defined by* (20)*,* (23)*,* (25) *and* (27) *satisfies the Gradient scheme coercivity, consistency and limit conformity properties in the sense of Definitions 3.1, 3.2 and 3.3.*

It results from Theorem 3.1 that the discrete variational formulation (16), or equivalentely the finite volume formulation (31)–(32) is well-posed. In addition, we have the following proposition regarding the error estimates.

Proposition 4.2 (Error Estimates)**.** *The VAG discretization defined by (20), (23), (25) and (27) satisfies the error estimates of Theorem 3.2 with* $\mathcal{S}_\mathcal{D}(u) + \mathcal{W}_\mathcal{D}(\boldsymbol{q}) \leq C(h_\mathcal{M} + h_\mathcal{G})$ *on matrix cell-wise, fracture face-wise and tunnel cell-wise smooth solutions, with* C *depending on the solution, the geometry, and on the mesh shape regularity parameter.*

Some remarks are in order.

Remark 4.2. *As stated in Remark 2.1, the limit model obtained for* $H_g \to +\infty$ *plays an important role in practical applications. The limit scheme obtained by passing to the limit* $H_g \to +\infty$ *in the VAG discretization just amount to restrict the discrete variational formulation (16) to the subspace*

$$X_\mathcal{D}^{\mathrm{c},0} = \{v_\mathcal{D} \in X_\mathcal{D}^0 \,|\, v_{\boldsymbol{s}} = \Pi_\mathcal{G} v_{\mathcal{D}_g}(x_{\boldsymbol{s}}) \text{ for all } \boldsymbol{s} \in \mathcal{V}_\Gamma\}.$$

It is remarkable that this limit scheme can be shown, using similar techniques, to satisfy coercivity, consistency and limit conformity properties (in the sense of the limit model) and to be first order accurate on piecewise smooth solutions of the limit model. The proof relies on a result similar to Lemma 7.4 for the Limit conformity property and on a stable lifting [46] for the Consistency property. This will be checked numerically in the following numerical Section.

Remark 4.3. *The Hybrid Mimetic Mixed (HMM) discretization is a family of first order polytopal discretizations based on face and cell unknowns including Mimetic Finite Difference (MFD) [11] and Hybrid Finite Volume (HFV) [22] schemes unified in [18]. It is extended in [7] to mixed-dimensional diffusion models including a network of fractures acting as drains. It can be further extended to our 3D-2D-1D mixed-dimensional model and shown to fit the Gradient Discretization Method of Section 3. This extension combines the HFV matrix and fracture function and gradient reconstruction operators defined in [7] with the discretization* $X_{\mathcal{D}_g}$, $\Pi_{\mathcal{D}_g}$, $\nabla_{\mathcal{D}_g}$ *defined by (19)-(23)-(25c) in the tunnel together with the following jump reconstruction operators:*

$$[\![v_\mathcal{D}]\!]_{\mathcal{D},\Gamma} = \sum_{\sigma\in\mathcal{F}_\Gamma} (v_\sigma - \Pi_\mathcal{G} v_{\mathcal{D}_g}(x_\sigma))\mathbf{1}_\sigma, \qquad [\![v_\mathcal{D}]\!]_{\mathcal{D},\Sigma_\Gamma} = \sum_{e\in\mathcal{E}_{\Sigma_\Gamma}} (v_e - \Pi_\mathcal{G} v_{\mathcal{D}_g}(x_e))\mathbf{1}_e.$$

The proof of the Limit conformity property relies on estimates similar to the ones of Lemma 7.4.

5 Numerical results

We provide an extensive numerical validation of the method on a set of model problems.

5.1 Convergence

We start by numerical experiments on a simplified geometry that demonstrate the convergence property of the method. We solve problem (31)–(32) using $\Omega_p = (0,1)^3$, $L = 1$, $\Omega_g = (0,L)\times\{(-\frac{1}{2},\frac{1}{2})\}$, $\omega = (-1,1)\times(0,1)$, $\omega_g = (-1,0)\times(0,1)$ and $\Gamma = (0,1)\times\{0\}\times(0,1)$.

We provide two analytical solutions for two different configurations where the porous medium is crossed by a single fracture. We consider three mesh families to discretize the porous medium Ω_p, two composed respectively of tetrahedral and regular cubic cells, and one composed of hexahedral cells, with are randomly perturbated nodes. On the tunnel side, we consider a regular segmentation of Ω_g. We monitor the following relative $L^2(\Omega_m)$-, $L^2(\Omega_f)$- and $L^2(\Omega_g)$-errors:

$$\epsilon_m^0 := \frac{\|u_p - \Pi_{\mathcal{D}_m} u_{\mathcal{D}_p}\|_{\Omega_m}}{\|u_p\|_{\Omega_m}}, \quad \epsilon_f^0 := \frac{\|\gamma_f u_p - \Pi_{\mathcal{D}_f} u_{\mathcal{D}_p}\|_{\Omega_f}}{\|\gamma_f u_p\|_{\Omega_f}}, \quad \epsilon_g^0 := \frac{\|u_g - \Pi_{\mathcal{D}_g} u_{\mathcal{D}_g}\|_{\Omega_g}}{\|u_g\|_{\Omega_g}},$$

together with the following relative $H^1(\Omega_m)$-, $H^1(\Omega_f)$- and $H^1(\Omega_g)$-errors:

$$\epsilon_m^1 := \frac{\|\nabla u_p - \nabla_{\mathcal{D}_m} u_{\mathcal{D}_p}\|_{\Omega_m}}{\|\nabla u_p\|_{\Omega_m}}, \quad \epsilon_f^1 := \frac{\|\nabla_\tau \gamma_f u_p - \nabla_{\mathcal{D}_f} u_{\mathcal{D}_p}\|_{\Omega_f}}{\|\nabla_\tau \gamma_f u_p\|_{\Omega_f}}, \quad \epsilon_g^1 := \frac{\|u_g' - \nabla_{\mathcal{D}_g} u_{\mathcal{D}_g}\|_{\Omega_g}}{\|u_g'\|_{\Omega_g}},$$

where $u = (u_p, u_g) \in V$ and $u_{\mathcal{D}} = (u_{\mathcal{D}_p}, u_{\mathcal{D}_g}) \in X_{\mathcal{D}}$ are the unique solutions of (9) and (31)-(32), respectively, with non homogeneous Dirichlet boundary conditions.

5.1.1 Longitudinal fracture

We consider the fracture $\Omega_f = \{\boldsymbol{x} = (x, y, z) \in \Omega_p \mid z = 1/2\}$ of constant thickness $d_f = 1$ intersecting the tunnel along $\Sigma_\Gamma = (0,1) \times \{0\} \times \{1/2\}$. We set the matrix diffusion tensor $\boldsymbol{\Lambda}_m = \boldsymbol{I}_3$, the fracture tangential diffusion tensor $\boldsymbol{\Lambda}_f = \boldsymbol{I}_2$, the tunnel diffusion $\Lambda_g = 1$, and the transfer coefficient $H_g = 1$. The exact solution is given by

$$u_p(\boldsymbol{x}) = \begin{cases} e^{x+y+z} + u_g(x) & \text{if } z \le 1/2 \\ e^{x+y+1-z} + u_g(x) & \text{if } z > 1/2 \end{cases}, \qquad u_g(x) = \sin(3x), \tag{33}$$

for all $\boldsymbol{x} \in \Omega_p$ and all $x \in (0,1)$. The source terms are given by

$$\begin{aligned} \mathrm{f}_m(\boldsymbol{x}) &= \begin{cases} -3e^{x+y+z} + 9\sin(3x) & \text{if } z \le 1/2 \\ -3e^{x+y+1-z} + 9\sin(3x) & \text{if } z > 1/2 \end{cases} && \forall \boldsymbol{x} \in \Omega_m, \\ \mathrm{f}_f(\boldsymbol{x}) &= 9\sin(3x) && \forall \boldsymbol{x} \in \Omega_f, \\ \mathrm{f}_g(x) &= 9\sin(3x) + 2e^x(1 - e^{1/2}) - e^{x+1/2} && \forall x \in (0,1). \end{aligned} \tag{34}$$

We set the number of tunnel mesh elements proportionally to $\sqrt[3]{|\mathcal{M}| + 1}$ so as to get non-conformities at the interface nodes between the porous medium and the tunnel in the sense of Remark 4.1. We display in Figure 5 the L^2- and H^1-error norms as a function of the meshsize $(h_{\mathcal{M}} + h_{\mathcal{G}})$. For the discretization errors measured in H^1-norms, we observe in the porous medium and in the tunnel convergence rates of order 1 on the tetrahedral meshes and a super-convergence of order 2 on the regular cubic meshes, except for the error along the tunnel as a result of the nonconformity. For the perturbed cubic meshes, we observe in the porous medium as in [7] a non smooth convergence due to the random perturbation of the porous medium nodes. However, as expected, the convergence rate is globally of order 1. For the discretization errors measured in L^2-norms, we observe a convergence of order 2 on the three meshes.

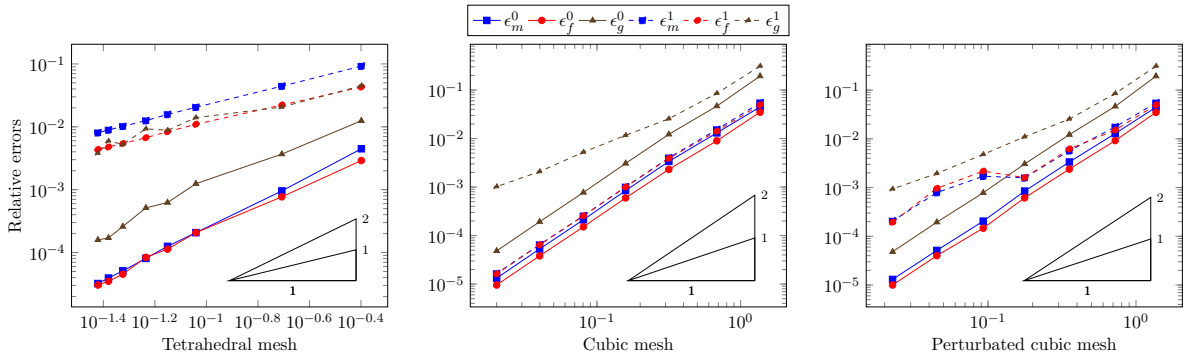

Figure 5: Errors vs. $(h_{\mathcal{M}} + h_{\mathcal{G}})$ on different meshes for the test case of Section 5.1.1.

5.1.2 Orthogonal fracture

We pursue by considering the fracture $\Omega_f = \{\boldsymbol{x} = (x, y, z) \in \Omega_p \mid x = 1/2\}$ of constant thickness $d_f = 1$ intersecting the tunnel along $\Sigma_\Gamma = \{1/2\} \times \{0\} \times (0, 1)$. We set the matrix diffusion tensor $\boldsymbol{\Lambda}_m = \boldsymbol{I}_3$, the fracture tangential diffusion tensor $\boldsymbol{\Lambda}_f = \boldsymbol{I}_2$, the tunnel diffusion $\Lambda_g = (6\cos(3/2))^{-1}(e^{3/2} - e^{1/2})$, and the transfer coefficient $H_g = 1$. The exact solution is given by

$$u_p(\boldsymbol{x}) = \begin{cases} e^{x+y+z} + u_g(x) & \text{if } x \leq 1/2 \\ e^{1-x+y+z} + u_g(x) & \text{if } x > 1/2 \end{cases}, \quad u_g(x) = \begin{cases} \sin(3x) & \text{if } x \leq 1/2 \\ \sin(3(1-x)) & \text{if } x > 1/2 \end{cases}, \tag{35}$$

for all $\boldsymbol{x} \in \Omega_p$ and all $x \in (0, 1)$. The source terms are given by

$$\begin{aligned} \mathrm{f}_m(\boldsymbol{x}) &= \begin{cases} -3e^{x+y+z} + 9\sin(3x) & \text{if } x \leq 1/2 \\ -3e^{1-x+y+z} + 9\sin(3(1-x)) & \text{if } x > 1/2 \end{cases} && \forall \boldsymbol{x} \in \Omega_m, \\ \mathrm{f}_f(\boldsymbol{x}) &= 6\cos(1/2) && \forall \boldsymbol{x} \in \Omega_f, \\ \mathrm{f}_g(x) &= \begin{cases} \Lambda_g 9\sin(3x) - e^x(e-1) & \text{if } x \leq 1/2 \\ \Lambda_g 9\sin(3(1-x)) - e^{1-x}(e-1) & \text{if } x > 1/2 \end{cases} && \forall x \in (0, 1). \end{aligned} \tag{36}$$

~~Also in this case~~As before, the number of tunnel mesh elements is proportional to $\sqrt[3]{|\mathcal{M}| + 1}$ and the meshes are nonconforming at the interface Γ between the porous medium and the tunnel. We display in Figure 6 the L^2- and H^1-error norms as a function of the meshsize $(h_{\mathcal{M}} + h_{\mathcal{G}})$. For the discretization errors measured in H^1-norms, we observe convergence rates of order 1 on the tetrahedral meshes and a super-convergence of order 2 on the regular cubic meshes, except for the error along the tunnel as a result of the nonconformity. For the perturbed cubic meshes, we observe the same behavior as the test case of Section 5.1.1 with a convergence rate globally of order 1. For the discretization errors measured in L^2-norms, we observe a convergence of order 2 on the three meshes.

5.1.3 Mesh conformity at the interface Γ

Next, we use conforming meshes at the interface Γ between the porous medium and the tunnel in the sense that $\{x_m, m \in \mathcal{V}_\mathcal{G}\} = \{x_{\boldsymbol{s}}, \boldsymbol{s} \in \mathcal{V}_\Gamma\}$. We consider the regular cubic mesh family and the two latter configurations with longitudinal fracture and exact solution given by (33), and orthogonal fracture with exact solution given by (35). We display in Figure 7

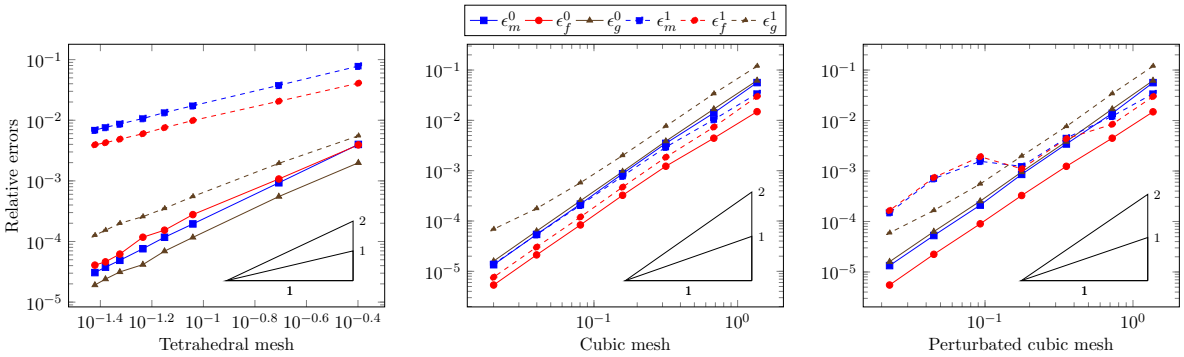

Figure 6: Errors vs. $(h_{\mathcal{M}} + h_{\mathcal{G}})$ on different meshes for the test case of Section 5.1.2.

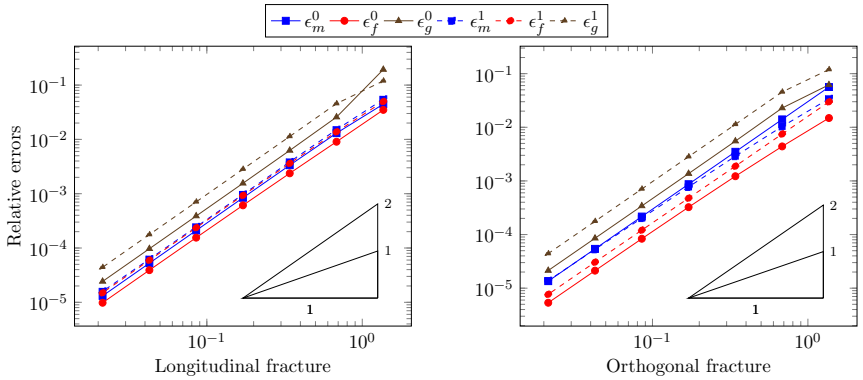

Figure 7: Errors vs. $(h_{\mathcal{M}} + h_{\mathcal{G}})$ on the regular cubic mesh family for the test case of Section 5.1.3.

the L^2- and H^1-error norms as function of the meshsize $(h_{\mathcal{M}} + h_{\mathcal{G}})$. In this case, we obtain superconvergence for all the H^1-error norms (including ϵ_g^1) independently of the fracture orientation; see, as a comparison, Figure 5 for the longitudinal fracture and Figure 6 for the orthogonal fracture.

5.1.4 One-sided mesh refinement

We now fix the meshsize of the porous medium or of the tunnel and proceed to a one-sided mesh refinement on the other region, nonconforming at the interface Γ. We consider the tetrahedral mesh family and the configuration with orthogonal fracture with exact solution given by (33). We first fix the tunnel meshsize $h_{\mathcal{G}} \in \{1/8, 1/32\}$ and display in Figure 8a the L^2- and H^1-error norms as function of the porous medium meshsize $h_{\mathcal{M}}$. As predicted by the theoretical results, the errors ϵ_g^0 and ϵ_g^1 in the tunnel do not increase when the porous medium mesh is refined. Then, we fix the porous medium meshsize $h_{\mathcal{M}} \in \{1.58 \cdot 10^{-1}, 7.32 \cdot 10^{-2}\}$ and display in Figure 8b the L^2- and H^1-error norms as function of the tunnel meshsize $h_{\mathcal{G}}$. Also in this case, the errors ϵ_m^0 and ϵ_m^1 in the matrix, and ϵ_f^0 and ϵ_f^1 in the fracture do not increase when we refine the tunnel mesh. Those two numerical results confirm that the errors are not sensitive to the ratio between the tunnel and porous medium meshsizes.

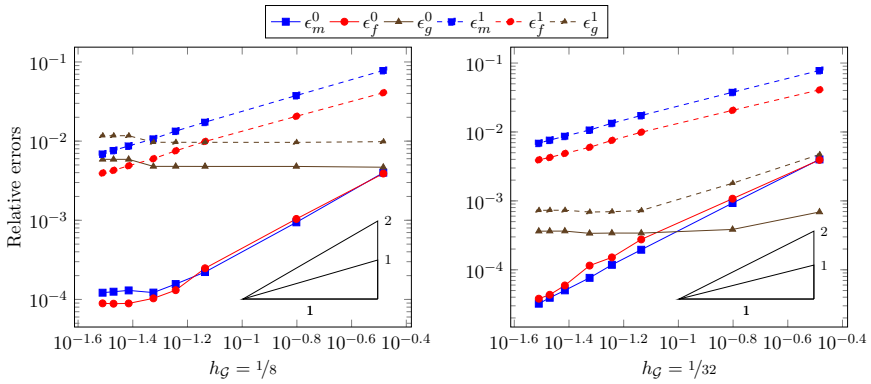

(a) Errors vs. $h_{\mathcal{M}}$ on the tetrahedral mesh family for the test case of Section 5.1.4 with $h_{\mathcal{G}} = 1/8$ (left) and $h_{\mathcal{G}} = 1/32$ (right).

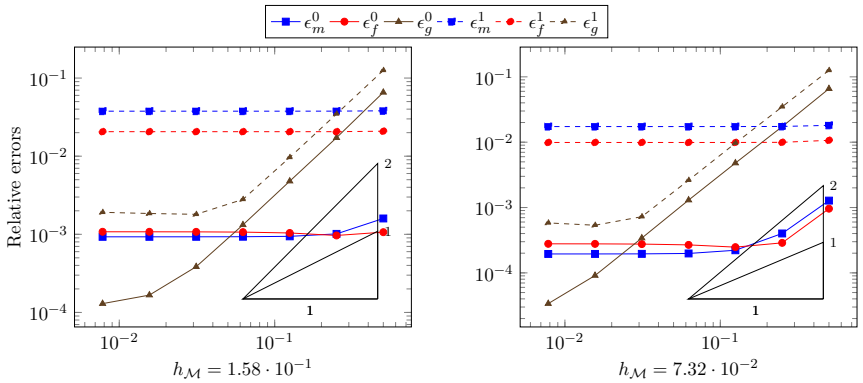

(b) Errors vs. $h_{\mathcal{G}}$ on the tetrahedral mesh family for the test case of Section 5.1.4 with $h_{\mathcal{M}} = 1.58 \cdot 10^{-1}$ (left) and $h_{\mathcal{M}} = 7.32 \cdot 10^{-2}$ (right).

Figure 8: Errors vs. $h_{\mathcal{M}}$ with fixed $h_{\mathcal{G}}$ (top) and vs. $h_{\mathcal{G}}$ with fixed $h_{\mathcal{M}}$ (bottom) for the test case of Section 5.1.4.

5.1.5 Limit case $H_g \to +\infty$.

Finally, we study the behavior of the discrete solution when $H_g \to +\infty$, that is we set $H_g = 10^i$ with $0 \le i \le 10$. As mentioned in Remark 2.1, this limit case amounts to imposing continuity of the solution at the interface in the sense that $\gamma_\Gamma u_p = u_g$ on Γ and $\gamma_{\Sigma_\Gamma}\gamma_f u_p = u_g$ on Σ_Γ. We consider the numerical experiment form [49, Section 2.2.5] that we recall here for the sake of completeness. The fracture is given by $\Omega_f = \{\boldsymbol{x} = (x,y,z) \in \Omega_p \mid x = 1/2\}$ of constant thickness $d_f = 1$ intersecting the tunnel along $\Sigma_\Gamma = \{1/2\} \times \{0\} \times (0,1)$. The matrix diffusion tensor is given by $\boldsymbol{\Lambda}_m = \boldsymbol{I}_3$, the fracture tangential diffusion tensor by $\boldsymbol{\Lambda}_f = \boldsymbol{I}_2$ and the tunnel diffusion coefficient by $\Lambda_g = (2\sin(1/2)e^{\cos(1/2)})^{-1}(\sin(1/2)e^{\cos(1/2)} - \sin(3/2) + \sin(1/2))$. The exact solution of the limit problem is given by

$$u_p(\boldsymbol{x}) = \begin{cases} y\cos(x+y+z) + e^{\cos(x+y)} & \text{if } x \le 1/2 \\ y\cos(1-x+y+z) + e^{\cos(1-x+y)} & \text{if } x > 1/2 \end{cases}, \qquad u_g(x) = u_p(x,0,0), \tag{37}$$

for all $\boldsymbol{x} \in \Omega_p$ and all $x \in (0,1)$. The source terms are given by

$$\begin{aligned} \forall \boldsymbol{x} \in \Omega_m, \quad \mathrm{f}_m(\boldsymbol{x}) &= \begin{cases} 2e^{\cos(x+y)}(\cos(x+y) - \sin^2(x+y)) & \text{if } x \le 1/2 \\ \quad +3y\cos(x+y+z) + 2\sin(x+y+z) & \\ 2e^{\cos(1-x+y)}(\cos(1-x+y) - \sin^2(1-x+y)) & \text{if } x > 1/2 \\ \quad +3y\cos(1-x+y+z) + 2\sin(1-x+y+z) & \end{cases}, \\ \forall \boldsymbol{x} \in \Omega_f, \quad \mathrm{f}_f(\boldsymbol{x}) &= e^{\cos(1/2+y)}(\cos(1/2+y) - \sin^2(1/2+y) \\ &\quad + y\cos(1/2+y+z) + 2\sin(1/2+y+z) \\ \forall x \in (0,1), \quad \mathrm{f}_g(x) &= \begin{cases} \Lambda_g e^{\cos(x)}(\sin(x) + \cos(x) - \sin^2(x)) & \text{if } x \le 1/2 \\ \quad +\sin(x) - \sin(x+1) & \\ \Lambda_g e^{\cos(1-x)}(\sin(1-x) + \cos(1-x) - \sin^2(1-x)) & \text{if } x > 1/2 \\ \quad +\sin(1-x) - \sin(2-x) & \end{cases} \end{aligned} \tag{38}$$

We consider meshes of fixed size that are nonconforming at the interface Γ. We display in Figure 9 the L^2- and H^1-error norms as a function of the transfer coefficient H_g on fixed tetrahedral and Cartesian meshes of respective size $h_\mathcal{M} = 3.84 \cdot 10^{-2}$ and $h_\mathcal{M} = 2.71 \cdot 10^{-2}$. On the tunnel side, we consider nonconforming meshes at the interface Γ and the tunnel meshsize is $h_\mathcal{G} = 8.93 \cdot 10^{-3}$ for the tetrahedral porous medium mesh and $h_\mathcal{G} = 1.28 \cdot 10^{-2}$ for the cartesian porous medium mesh. In Figure 10, we fix $H_g = 10^{10}$ and display the value of the L^2- and H^1-error norms as a function of the meshsize $(h_\mathcal{M} + h_\mathcal{G})$ on the tetrahedral and cartesian mesh families, and set the number of tunnel mesh elements proportionally to $\sqrt[3]{|\mathcal{M}|+1}$ so as to get nonconformities at the interface nodes between the porous medium and the tunnel. These results confirm as stated in Remark 4.2 that the limit scheme has optimal convergence rates for the solutions of the limit model of Remark 2.1.

5.2 Application to a drying model

We extend the Finite Volume formulation (31)–(32) to the following drying model coupling the Richards equation in the fractured porous medium with the convection diffusion of the vapor molar fraction along the tunnel; see also [41, 47, 16]. The physical domain represents a quarter of a cylinder with an axial hole along the x-axis corresponding to the excavated tunnel. Recalling definitions of Section 2.1, the porous medium is defined as $\Omega_p = (0,L) \times (\omega \setminus$

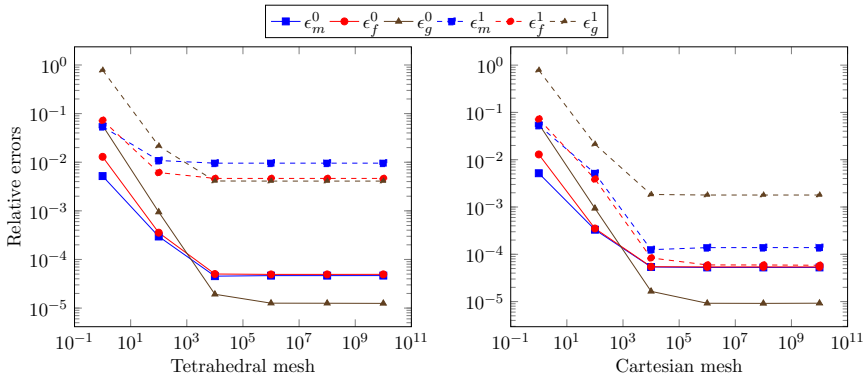

Figure 9: Errors vs. H_g on fixed tetrahedral (left) and cartesian (right) meshes for the test case of Section 5.1.5 with fixed $h_{\mathcal{M}}$ and $h_{\mathcal{G}}$.

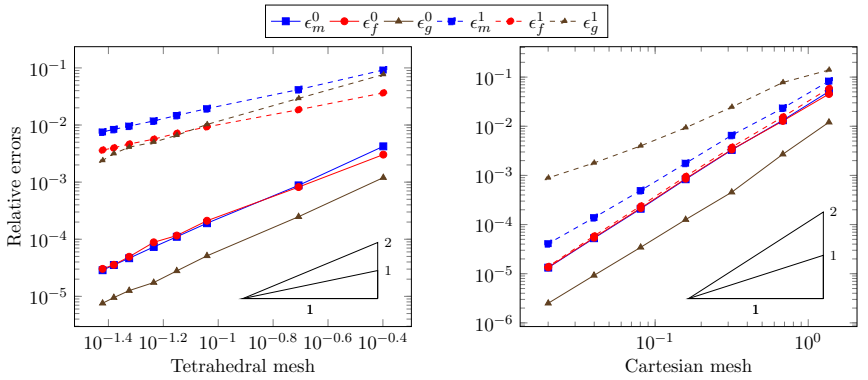

Figure 10: Errors vs. $(h_{\mathcal{M}} + h_{\mathcal{G}})$ on different meshes for the test case of Section 5.1.5 with $H_g = 10^{10}$.

$\overline{\omega_g}$) and the tunnel as $\Omega_g = (0, L) \times \{\boldsymbol{x}_g\}$, with $L = 20$, $\omega = \{(y, z) \in \mathbb{R}_+^* \times \mathbb{R}_+^* \mid \sqrt{y^2 + z^2} < 12.5\}$, $\omega_g = \{(y, z) \in \mathbb{R}_+^* \times \mathbb{R}_+^* \mid \sqrt{y^2 + z^2} < 2.5\}$ and $\boldsymbol{x}_g = (0, 0)$. The fracture network is composed of 10 slighlty inclined fractures, evenly distributed along the x-axis and at equal distance from each other. The fluxes at the interfaces $\Gamma = (0, L) \times (\partial\omega_g \cap \omega)$ between the porous medium and the tunnel account for the turbulent boundary layer of the vapor molar fraction.

We denote by $p^l : (0, t_F) \times \Omega_p \to \mathbb{R}$ the liquid pressure in the porous medium and by $c^g : (0, t_F) \times \Omega_g \to \mathbb{R}$ the vapor molar fraction in the tunnel with $t_F = 100$ years. Let $\mathrm{rt} \in \{m, f\}$ denote the matrix or fracture rocktype. The liquid saturation as a function of the liquid pressure is denoted by $S^l_{\mathrm{rt}} : \mathbb{R} \to \mathbb{R}$ and the liquid relative permeability as a function of the liquid saturation by $k^l_{r,\mathrm{rt}} : \mathbb{R} \to \mathbb{R}$. The liquid molar density is fixed to $\zeta^l = 10^3/(1.8 \cdot 10^{-2})$ mol.m^{-3} and the liquid dynamic viscosity to $\mu^l = 10^{-3}$ Pa·s. Using the fixed gas pressure $p^g = 10^5$ Pa and temperature $T = 303$ K, the gas molar density is set to $\zeta^g = p^g/RT$ mol.m^{-3} with $R = 8.314$ J.mol^{-1}.K^{-1}. In the matrix, the permeability is assumed isotropic and set to $\Lambda_m = 5 \cdot 10^{-20}$ m^2 and the porosity is $\phi_m = 0.15$. The fractures are assumed to be filled only by the gas and liquid phases, the porosity is hence set to $\phi_f = 1$, the fracture aperture to $d_f = 1$ mm and the tangential permeability is given by the Poiseuille law $\Lambda_f = \frac{(d_f)^2}{12}$. In the tunnel, we denote by $v = 0.1$ m.s^{-1} the constant gas velocity, by $\Lambda_g = 2 \cdot 10^{-3}$ m^2.s^{-1} the turbulent diffusion coefficient, and by $H_g = 1.46 \cdot 10^{-2}$ mol.m^{-2}.s^{-1} the molar convective transfer coefficient computed from the Dittus Bolter correlation. The function $\overline{c} : \mathbb{R} \to \mathbb{R}$ computes the vapor molar fraction at the interface Γ and Σ_Γ as a function of the liquid pressure. It is based on the liquid-gas thermodynamical equilibrium for water assuming the vaporization of the liquid phase at the interface between the porous medium and the tunnel:

$$\overline{c}(p^l) \coloneqq \frac{p_{sat}(T)}{p^g} e^{-(p^g - p^l)/(\zeta^l RT)},$$

with $p_{sat}(T) = 1.013 \cdot 10^5 \exp(13.7 - 5120/T)$ Pa the saturated vapor pressure.

We consider the following mixed-dimensional model coupling the molar conservation equations and constitutive laws

$$\begin{cases} \phi_m \zeta^l \partial_t(S^l_m(p^l)) + \mathrm{div}(\boldsymbol{q}_m) = 0 & \text{in } (0, t_F) \times \Omega_m, \\ d_f \phi_f \zeta^l \partial_t(S^l_f(\gamma_f p^l)) + r_f(\boldsymbol{q}_p) = 0 & \text{in } (0, t_F) \times \Omega_f, \\ \zeta^g |\omega_g| \partial_t c^g + r_g(\boldsymbol{q}) = 0 & \text{in } (0, t_F) \times \Omega_g, \\ \boldsymbol{q}_m = -\dfrac{\zeta^l}{\mu^l} k^l_{\mathrm{r},m}(S^l_m(p^l)) \boldsymbol{\Lambda}_m \nabla p^l & \text{in } (0, t_F) \times \Omega_m, \\ \boldsymbol{q}_f = -d_f \dfrac{\zeta^l}{\mu^l} k^l_{\mathrm{r},f}(S^l_f(\gamma_f p^l)) \boldsymbol{\Lambda}_f \nabla_\tau \gamma_f p^l & \text{in } (0, t_F) \times \Omega_f, \\ q_g = \zeta^g |\omega_g| (v c^g - \Lambda_g \partial_x c^g) & \text{in } (0, t_F) \times \Omega_g, \\ \boldsymbol{q}_m \cdot \boldsymbol{n}_\Gamma = H_g(\overline{c}(\gamma_\Gamma p^l) - c^g) & \text{on } (0, t_F) \times \Gamma, \\ \boldsymbol{q}_f \cdot \boldsymbol{n}_{\Sigma_\Gamma} = d_f H_g(\overline{c}(\gamma_{\Sigma_\Gamma} \gamma_f p^l) - c^g) & \text{on } (0, t_F) \times \Sigma_\Gamma, \end{cases} \tag{39}$$

where $\boldsymbol{n}_{\Omega_m}$ (resp. $\boldsymbol{n}_{\Omega_f}$) is the unit vector normal to $\partial\Omega_m$ (resp. $\partial\Omega_f$) and is oriented outward to Ω_m (resp. Ω_f). Initial conditions $p^l(t = 0) = 4 \cdot 10^6$ Pa in Ω_m, $p^l(t = 0) = p^g$ Pa on Γ, $p^l(t = 0) = p^g$ Pa in Ω_f, $p^l(t = 0) = p^g$ Pa on Σ_Γ, and $c^g(t = 0) = \frac{1}{2}\frac{p_{sat}(T)}{p^g}$ mol.m^{-3} in Ω_g along with the following Dirichlet and Neumann boundary conditions $p^l = 4 \cdot 10^6$ Pa on $(0, t_F) \times \Gamma_D$, $c^g = \frac{1}{2}\frac{p_{sat}(T)}{p^g}$ mol.m^{-3} on $(0, t_F) \times \partial\Omega_g^D$,

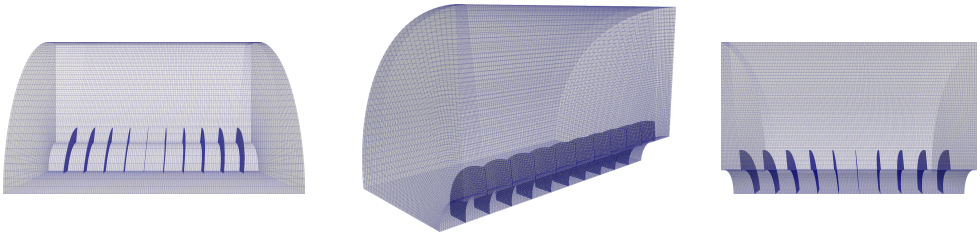

Figure 11: Parallelepiped mesh used for the test case of Section 5.2.

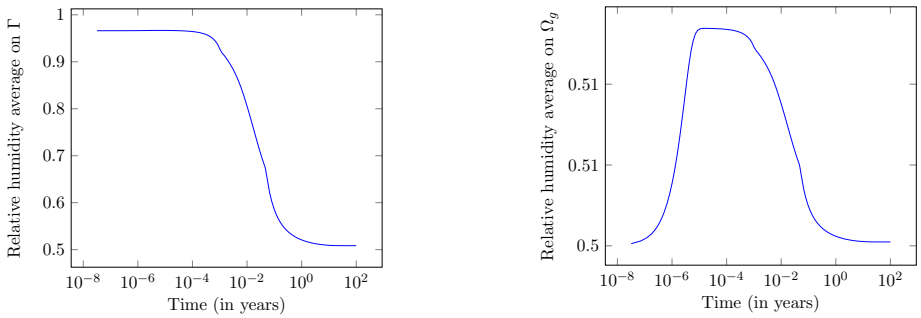

(a) Relative humidity average on Γ vs. time (b) Relative humidity average on Ω_g vs. time

Figure 12: Relative humidity average on the interface Γ (left) on the tunnel Ω_g (right) vs. time (in years).

$\boldsymbol{q}_m \cdot \boldsymbol{n}_{\Omega_m} = 0$ on $(0, t_F) \times \Gamma_N$, $\boldsymbol{q}_f \cdot \boldsymbol{n}_{\Omega_f} = 0$ on $(0, t_F) \times \Sigma_N$ and $q_g = 0$ on $(0, t_F) \times \partial\Omega_g^N$ close the problem, where $\Gamma_D := \{\boldsymbol{x} \in \partial\Omega_p \mid \sqrt{y^2 + z^2} = 12.5\}$, $\Gamma_N := \{\boldsymbol{x} \in \partial\Omega_p \mid x \in \{0, 20\}\}$, $\partial\Omega_g^D := (0, 0, 0)$ and $\partial\Omega_g^N := (L, 0, 0)$.

The spacial discretization is based on the Finite Volume formulation (31) combined with an upwind approximation of the mobilities in the matrix and fracture Richards equations and of the convective term in the tunnel. A standard implicit Euler method with an adaptive time step is used to discretize in time. The initial time step is set to 1 second and increases by 20% for each convergence of the Newton's algorithm. The simulation required 190 time steps, and the Newton's algorithm never failed to converge with an average of 4.2 iterations by time step. We display in Figure 11 the mesh used to discretize the geometry, composed of 354354 parallelepipedic elements and where each fracture is composed of 585 mesh faces. We depict in Figure 12a and 12b the relative humidity average as a function of time on Γ and in Ω_g, respectively, in Figure 13 the relative humidity on Γ at different time, in Figure 14 the vapor molar fraction on $\Omega_g$at different time, and in Figure 15 the gas saturation in the matrix and the fracture network at different time. We can identify four stages of drying: (i) the first stage appears at the early stage of the simulation, where the relative humidity at the interface is roughly constant and close to 1; (ii) in the second stage, the gas is entering the matrix and the molar flow rate on the interface decrease but the fracture stay saturated; (iii) the third stage is very short and corresponds to the desaturation of fractures that causes a quick drop of humidity; (iv) the last stage corresponds to the gas spreading into the matrix leading to convergence towards the steady state with a small but nonzero molar flow rate at the interface and a relative humidity close to its initial value.

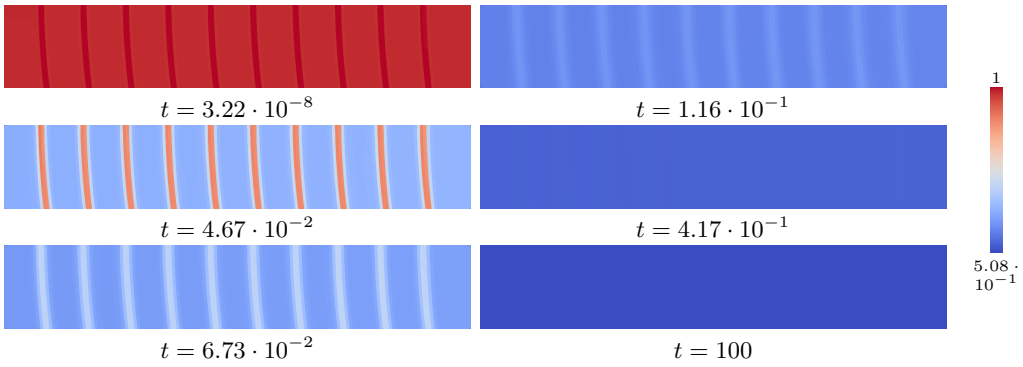

Figure 13: Evolution of the relative humidity on Γ (time scale expressed in years).

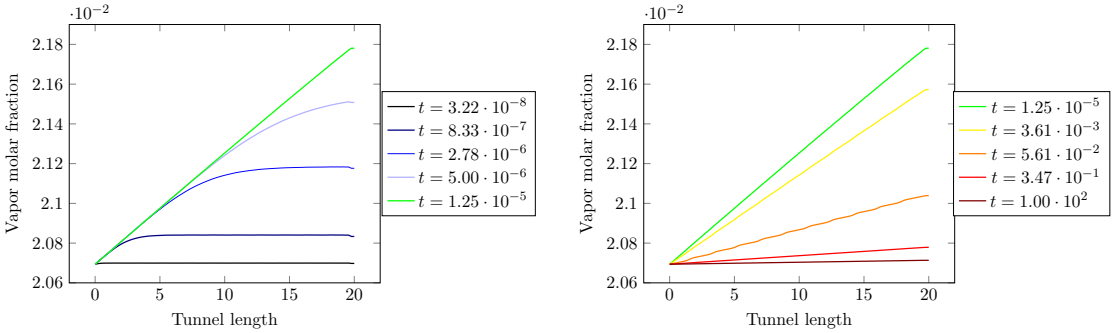

(a) Increasing phase

(b) Decreasing phase

Figure 14: Evolution of the vapor molar fraction along the tunnel Ω_g (time scale expressed in years).

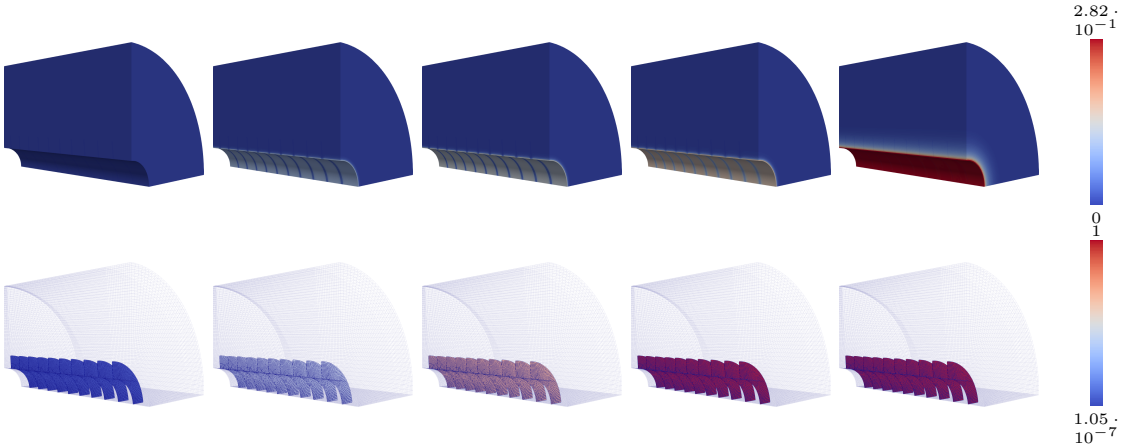

Figure 15: Evolution of the gas saturation in the matrix (top) and the fracture network (right). Displayed times are 0, $3.21 \cdot 10^{-8}$, $2.25 \cdot 10^{-2}$, $3.89 \cdot 10^{-2}$, $6.73 \cdot 10^{-2}$, 100 (in years).

6 Conclusion

We introduced a mixed-dimensional 3D-2D-1D diffusive model accounting for the coupling between an embedding matrix domain and embedded fracture and tubular networks. The reduction of dimension for the tubular network is based on a resolved interface formulation. The transmission conditions assume the continuity of the potential across fractures and Robin type conditions across the interface Γ between the 3D-2D fractured porous medium and the 1D centerline of the tubular network.

The discretization of the mixed-dimensional model is formulated in the abstract GD framework accounting for both conforming and non conforming approximations. It allows to derive stability and error estimates assuming that the GD verifies generic coercivity, consistency and limit conformity properties. The VAG scheme, accounting for unstructured polyhedral meshes, was previously developed for Discrete Fracture Matrix models. It is here extended to the coupling with the 1D model using a 1D Finite Element discretization possibly non conforming with the VAG discretization at the interface Γ. It is based on a simple interpolation operator and a lumping of the VAG basis functions at the tubular interface. Although the presentation assumes for readability a single cylindrical tube intersected by the fracture network, the framework and the discretization can be readily extended to more general tubular networks based on the definition of a surjective mapping from the tubular network interface to its centerline. The VAG scheme is proven to meet the GD properties and provide first order error estimates on piece-wise smooth solutions. It is also asymptotic preserving in the limit of large transfer coefficients. These results are confirmed numerically on analytical solutions using a simplified geometry based on a plane interface. Exploiting the VAG equivalent Finite Volume formulation and the local flux expression, the discretization is extended to a nonlinear drying model coupling the Richards equation in the fractured porous medium to the convection diffusion of the vapor molar fraction along the 1D domain. It is successfully applied to simulate the drying process between an operating tunnel and a radioactive waste storage rock with explicit representation of the fractures in the excavated damaged zone.

7 Proof of main results

This section gather technical proofs of the main results stated in Section 2 followed by the ones of Section 4.4.

7.1 Proofs of Section 2

We start by proving the Lemma 2.2.

Proof of Lemma 2.2. We first prove that $C_W^\infty \subset W$.

Let us define the two sides $\pm$ of the fracture network and the corresponding unit normal vectors $\boldsymbol{n}^\pm$ on Ω_f oriented outward to the sides $\pm$. For all $\boldsymbol{q}_m \in H(\mathrm{div};\Omega_m)$, we denote by $\gamma_{\boldsymbol{n}^\pm}\boldsymbol{q}_m$ the two normal traces on the fracture network Ω_f.

Let $\boldsymbol{q} \in C_W^\infty$, setting

$$r_f(\boldsymbol{q}_p) = \mathrm{div}_\tau(\boldsymbol{q}_f) - \gamma_{\boldsymbol{n}^+}\boldsymbol{q}_m + \gamma_{\boldsymbol{n}^-}\boldsymbol{q}_m, \tag{40}$$

with div_τ denoting the tangential divergence operator on Ω_f, using the density result from [7, Proposition 3] and an integration by part formula, one has that $\boldsymbol{q}_p \in W^p$. Then, let

$r_g(\boldsymbol{q}) \in \mathcal{D}'(\Omega_g)$ be defined by

$$\int_{\Omega_g} r_g(\boldsymbol{q})\varphi \mathrm{d}x = -\int_{\Omega_g} q_g \varphi' \mathrm{d}x - \int_\Gamma (\boldsymbol{q}_m \cdot \boldsymbol{n}_\Gamma)\varphi \, \mathrm{d}\tau(\boldsymbol{x}) - \int_{\Sigma_\Gamma} (\boldsymbol{q}_f \cdot \boldsymbol{n}_{\Sigma_\Gamma})\varphi \, \mathrm{d}l(\boldsymbol{x}), \tag{41}$$

for all $\varphi \in C_c^\infty(\Omega_g)$, using implicitly the extension $\varphi(\boldsymbol{x}) = \varphi(x)$ for all $\boldsymbol{x} = (x, y, z) \in \Gamma$. From the definition (5) of C_W^∞, we deduce that $r_g(\boldsymbol{q}) \in L^2(\Omega_g)$. Using that $C_c^\infty(\Omega_g)$ is dense in $H_0^1(\Omega_g)$, it results that $\boldsymbol{q}$ and $r_g(\boldsymbol{q})$ satisfy (3).

We now prove that C_W^∞ is dense in W. Let $\xi \in W'$. From the Riesz representation theorem, there exist $a_m \in L^2(\Omega_p)$, $\boldsymbol{A}_m \in L^2(\Omega_p)^3$, $a_f \in L^2(\Omega_f)$, $\boldsymbol{A}_f \in L^2(\Omega_f)^2$, $a_g \in L^2(\Omega_g)$, $A_g \in L^2(\Omega_g)$, and $b_m \in L^2(\Gamma)$, $b_f \in L^2(\Sigma_\Gamma)$ such that for all $\boldsymbol{q} \in W$

$$\begin{aligned}\langle \xi, \boldsymbol{q}\rangle_{W',W} = &\int_{\Omega_m} (\boldsymbol{q}_m \cdot \boldsymbol{A}_m + a_m \, \mathrm{div}(\boldsymbol{q}_m))\mathrm{d}\boldsymbol{x} + \int_{\Omega_f} (\boldsymbol{q}_f \cdot \boldsymbol{A}_f + r_f(\boldsymbol{q})a_f)\mathrm{d}\tau(\boldsymbol{x}) \\ &+ \int_{\Omega_g} (q_g A_g + r_g(\boldsymbol{q})a_g)dx - \int_\Gamma (\boldsymbol{q}_m \cdot \boldsymbol{n})b_m \mathrm{d}\tau(\boldsymbol{x}) - \int_{\Sigma_\Gamma} (\boldsymbol{q}_f \cdot \boldsymbol{n}_{\Sigma_\Gamma})b_f \mathrm{d}l(\boldsymbol{x}).\end{aligned} \tag{42}$$

Let us assume that $\langle \xi, \boldsymbol{q}\rangle_{W',W} = 0$ for all $\boldsymbol{q} \in C_W^\infty$. Then, the density of C_W^∞ in W is obtained if this imply that $\langle \xi, \boldsymbol{q}\rangle_{W',W} = 0$ for all $\boldsymbol{q} \in W$. From the definition of W it suffices to prove that $a_m \in V_0^p$, $\boldsymbol{A}_m = \nabla a_m$, $a_f = \gamma_f a_m$, $\boldsymbol{A}_f = \nabla_\tau a_f$, $a_g \in H_0^1(\Omega_g)$, $A_g = a_g'$, $b_m = \gamma_\Gamma a_m - a_g$ and $b_f = \gamma_{\Sigma_\Gamma} a_m - a_g$. Using [7, Lemma 8], it holds that $a_m \in H^1(\Omega_p)$ with $a_m = 0$ on Γ_D, $a_f \in H^1(\Omega_f)$ with $a_f = 0$ on Σ_D, $\boldsymbol{A}_m = \nabla a_m$, $a_f = \gamma_f a_m$ and $\boldsymbol{A}_f = \nabla_\tau a_f$. Taking $\boldsymbol{q} = (\boldsymbol{0}, \boldsymbol{0}, q_g)$ in (42) for any $q_g \in C^\infty(\overline{\Omega}_g)$, it follows that $a_g \in H_0^1(\Omega_g)$ with $A_g = a_g'$. Next, setting $\boldsymbol{q} = (\boldsymbol{q}_m, \boldsymbol{0}, 0)$ in (42) for any $\boldsymbol{q}_m$ in $C^\infty(\overline{\Omega}_m)^3$, it follows from the definitions (41) and (40) of $r_g(\boldsymbol{q})$ and $r_f(\boldsymbol{q}_p)$ that

$$\int_\Gamma (\boldsymbol{q}_m \cdot \boldsymbol{n})(\gamma_\Gamma a_m - a_g - b_m)\mathrm{d}\tau(\boldsymbol{x}) = 0,$$

which implies that $b_m = \gamma_\Gamma a_m - a_g$. Finally, setting $\boldsymbol{q} = (\boldsymbol{0}, \boldsymbol{q}_f, 0) \in C_W^\infty$ in (42), recalling the definitions (40) and (41) of, respectively, $r_f(\boldsymbol{q})$ and $r_g(\boldsymbol{q}_p)$, it follows that

$$\int_{\Sigma_\Gamma} (\boldsymbol{q}_f \cdot \boldsymbol{n}_{\Sigma_\Gamma})(\gamma_{\Sigma_\Gamma} a_f - a_g - b_f)\mathrm{d}l(\boldsymbol{x}) = 0,$$

which implies $b_f = \gamma_{\Sigma_\Gamma} a_f - a_g$, concluding the proof. □

7.2 Proofs of Section 4.4

7.2.1 Preliminary results

We first recall approximation properties of the interpolators $\Pi_{\mathcal{T}} \mathcal{P}_{\mathcal{D}_p}$ and $\Pi_{\mathcal{G}} \mathcal{P}_{\mathcal{D}_g}$, with $\Pi_{\mathcal{T}}$ and $\Pi_{\mathcal{G}}$ defined in (24), and $\mathcal{P}_{\mathcal{D}_p}$ and $\mathcal{P}_{\mathcal{D}_g}$ in (22), stemming from the classical conforming finite element approximation theory; see e.g. [21].

Lemma 7.1 (Approximation properties of $\Pi_{\mathcal{T}}$ and $\Pi_{\mathcal{G}}$)**.** *For all $(\varphi_p, \varphi_g) \in \mathcal{C}^2(\overline{\Omega_p}) \times \mathcal{C}^2(\overline{\Omega}_g)$, there exist two positive constants $C_{\mathcal{T}}(\varphi_p)$ and $C_{\mathcal{G}}(\varphi_g)$ depending only on, respectively, φ_p and the mesh regularity parameter, and φ_g, such that it holds*

$$\begin{aligned}&\|\varphi_p - \Pi_{\mathcal{T}} \mathcal{P}_{\mathcal{D}_p} \varphi_p\|_{\Omega_m} + \|\gamma_f \varphi_p - \gamma_f \Pi_{\mathcal{T}} \mathcal{P}_{\mathcal{D}_p} \varphi_p\|_{\Omega_f} \\ &+ h_{\mathcal{M}} \left(\|\nabla \varphi_p - \nabla \Pi_{\mathcal{T}} \mathcal{P}_{\mathcal{D}_p} \varphi_p\|_{\Omega_m} + \|\nabla_\tau \gamma_f \varphi_p - \nabla_\tau \gamma_f \Pi_{\mathcal{T}} \mathcal{P}_{\mathcal{D}_p} \varphi_p\|_{\Omega_f} \right) \le C_{\mathcal{T}}(\varphi_p) h_{\mathcal{M}}^2, \qquad (43a) \\ &\|\varphi_g - \Pi_{\mathcal{G}} \mathcal{P}_{\mathcal{D}_g} \varphi_g\|_{\Omega_g} + h_{\mathcal{G}} \|\varphi_g' - (\Pi_{\mathcal{G}} \mathcal{P}_{\mathcal{D}_g} \varphi_g)'\|_{\Omega_g} \le C_{\mathcal{G}}(\varphi_g) h_{\mathcal{G}}^2. \qquad (43b)\end{aligned}$$

We then recall approximation properties obtained in [9, Lemma 3.4] of the operators $\Pi_{\mathcal{D}_m}$, $\Pi_{\mathcal{D}_f}$ and $\Pi_{\mathcal{D}_g}$ defined in (23), noticing that the shape regularity of $\mathcal{T}$ implies the shape regularity of the triangular submesh of Ω_f.

Lemma 7.2 (Approximation properties of $\Pi_{\mathcal{D}_m}$, $\Pi_{\mathcal{D}_f}$ and $\Pi_{\mathcal{D}_g}$)**.** *There exists three positive constants C_m, C_f, and C_g depending only on the mesh regularity parameter such that, for all $v_{\mathcal{D}} = (v_{\mathcal{D}_p}, v_{\mathcal{D}_g}) \in X_{\mathcal{D}}$, it holds*

$$\|\Pi_{\mathcal{D}_m} v_{\mathcal{D}_p} - \Pi_{\mathcal{T}} v_{\mathcal{D}_p}\|_{\Omega_m} \le C_m h_{\mathcal{M}} \|\nabla_{\mathcal{D}_m} v_{\mathcal{D}_p}\|_{\Omega_m} \tag{44a}$$

$$\|\Pi_{\mathcal{D}_f} v_{\mathcal{D}_p} - \gamma_f \Pi_{\mathcal{T}} v_{\mathcal{D}_p}\|_{\Omega_f} \le C_f h_{\mathcal{M}} \|\nabla_{\mathcal{D}_f} v_{\mathcal{D}_p}\|_{\Omega_f} \tag{44b}$$

$$\|\Pi_{\mathcal{D}_g} v_{\mathcal{D}_g} - \Pi_{\mathcal{G}} v_{\mathcal{D}_g}\|_{\Omega_g} \le C_g h_{\mathcal{G}} \|\nabla_{\mathcal{D}_g} v_{\mathcal{D}_g}\|_{\Omega_g} \tag{44c}$$

We also state the following Lemma on the equivalence between two gradient discretizations; see [7, Lemma 1] for a proof.

Lemma 7.3. *Let $\mathcal{D}$ be the gradient discretization defined by (20), (23), (25) and (27), and $\widetilde{\mathcal{D}}$ be the gradient discretization defined by (20), (24), (25) and (27). Then, it results from (44) that for any shape regular family of meshes, each property (coercivity, consistency or limit conformity) for $\mathcal{D}$ is equivalent to the same property for $\widetilde{\mathcal{D}}$. In addition, from (44), the estimates of the consistency and limit-conformity terms differ only up a first order term $h_{\mathcal{M}} + h_{\mathcal{G}}$.*

7.2.2 Proofs of discrete results

From now on and for any mesh element $X \in \mathcal{M} \cup \mathcal{F} \cup \mathcal{E}$, we define $\underline{x}_X := \min\{x_{\boldsymbol{s}} \mid \boldsymbol{x}_{\boldsymbol{s}} = (x_{\boldsymbol{s}}, y_{\boldsymbol{s}}, z_{\boldsymbol{s}}) \text{ for all } \boldsymbol{s} \in \mathcal{V}_X\}$ and $\overline{x}_X := \max\{x_{\boldsymbol{s}} \mid \boldsymbol{x}_{\boldsymbol{s}} = (x_{\boldsymbol{s}}, y_{\boldsymbol{s}}, z_{\boldsymbol{s}}) \text{ for all } \boldsymbol{s} \in \mathcal{V}_X\}$.

The following key Lemma compares the $\mathbb{P}_1$ Finite Element and piecewise constant reconstructions of any $v_{\mathcal{D}_g} \in X_{\mathcal{D}_g}$ on the interfaces Γ and Σ_Γ.

Lemma 7.4. *For all $v_{\mathcal{D}_g} \in X_{\mathcal{D}_g}$, one has the following estimates*

$$\|\Pi_{\mathcal{G}} v_{\mathcal{D}_g} - \sum_{\boldsymbol{s} \in \mathcal{V}_\Gamma} \Pi_{\mathcal{G}} v_{\mathcal{D}_g}(x_{\boldsymbol{s}}) \mathbf{1}_{\sigma_{\Gamma,\boldsymbol{s}}}\|_\Gamma \le C_\Gamma h_{\mathcal{M}} \|\nabla_{\mathcal{D}_g} v_{\mathcal{D}_g}\|_{\Omega_g}, \tag{45a}$$

$$\|\Pi_{\mathcal{G}} v_{\mathcal{D}_g} - \sum_{\boldsymbol{s} \in \mathcal{V}_{\Sigma_\Gamma}} \Pi_{\mathcal{G}} v_{\mathcal{D}_g}(x_{\boldsymbol{s}}) \mathbf{1}_{e_{\Sigma_\Gamma,\boldsymbol{s}}}\|_{\Sigma_\Gamma} \le C_{\Sigma_\Gamma} h_{\mathcal{M}} \|\nabla_{\mathcal{D}_g} v_{\mathcal{D}_g}\|_{\Omega_g}, \tag{45b}$$

with C_Γ and C_{Σ_Γ} two positive constants independant of $h_{\mathcal{M}}$ and $h_{\mathcal{G}}$.

Proof of Lemma 7.4. We first prove (45a). Let us consider the points $(\widetilde{x}_k)_{0 \le k \le N_\Gamma} \in \overline{\Omega_g}^{N_\Gamma+1}$ such that $\widetilde{x}_0 = 0$, $\widetilde{x}_{N_\Gamma} = L$, $\widetilde{x}_{k+1} - \widetilde{x}_k = h_{\mathcal{M}}$ for all $k \in \{0, \cdots, N_\Gamma - 2\}$, and $\widetilde{x}_{N_\Gamma} - \widetilde{x}_{N_\Gamma - 1} \le h_{\mathcal{M}}$. We estimate the left-hand side of (45a) using the overlapping decomposition of Γ defined by $\cup_{k=0}^{N_\Gamma-2} ((\widetilde{x}_k, \widetilde{x}_{k+2}) \times \partial\omega_g)$. We define the set of faces $\mathcal{F}_\Gamma^k = \{\sigma \in \mathcal{F}_\Gamma \,|\, \sigma \subset [\widetilde{x}_k, \widetilde{x}_{k+2}] \times \partial\omega_g\}$ for all $k \in \{0, \cdots, N_\Gamma - 2\}$, and set $w = \Pi_{\mathcal{G}} v_{\mathcal{D}_g}$ for some $v_{\mathcal{D}_g} \in X_{\mathcal{D}_g}$, and for all $k \in \{0, \cdots, N_\Gamma - 2\}$, by $\overline{w}_k = \max_{x \in I_k} w(x)$ and $\underline{w}_k = \min_{x \in I_k} w(x)$ with $I_k = \{\widetilde{x}_k, \widetilde{x}_{k+2}\} \cup \{(x_m)_{m \in \mathcal{V}_\mathcal{G}} \mid \widetilde{x}_k < x_m < \widetilde{x}_{k+2}\}$. Then, it holds

$$\sum_{\sigma \in \mathcal{F}_\Gamma} \|w - \sum_{\boldsymbol{s} \in \mathcal{V}_\Gamma} w(x_{\boldsymbol{s}}) \mathbf{1}_{\sigma_{\Gamma,\boldsymbol{s}}}\|_\sigma^2 \le \sum_{k=0}^{N_\Gamma-2} \sum_{\sigma \in \mathcal{F}_\Gamma^k} |\sigma| \, (\overline{w}_k - \underline{w}_k)^2 \le \sum_{k=0}^{N_\Gamma-2} \sum_{\sigma \in \mathcal{F}_\Gamma^k} |\sigma| \left(\int_{\widetilde{x}_k}^{\widetilde{x}_{k+2}} |w'(x)| \mathrm{d}x \right)^2. \tag{46}$$

Finally, using a Cauchy-Schwarz inequality in (46) together with the fact that $|\widetilde{x}_{k+2} - \widetilde{x}_k| \le 2h_{\mathcal{M}}$ and $\sum_{\sigma\in\mathcal{F}_\Gamma^k}|\sigma| \le 2h_{\mathcal{M}}|\partial\omega_g|$, we obtain

$$\sum_{\sigma\in\mathcal{F}_\Gamma}\|w - \sum_{\boldsymbol{s}\in\mathcal{V}_\Gamma} w(x_{\boldsymbol{s}})\mathbf{1}_{\sigma_{\Gamma,\boldsymbol{s}}}\|_\sigma^2 \le (2h_{\mathcal{M}})^2|\partial\omega_g|\sum_{k=0}^{N_\Gamma-2}\int_{\widetilde{x}_k}^{\widetilde{x}_{k+2}}|w'(x)|^2\mathrm{d}x \le 2(2h_{\mathcal{M}})^2|\partial\omega_g|\int_{\Omega_g}|w'(x)|^2\mathrm{d}x,$$

and the result follows from the definition (25c) of $\nabla_{\mathcal{D}_g}$.

We now prove (45b). Let $i\in\mathcal{I}_f$ be a fracture index and $w = \Pi_{\mathcal{G}}v_{\mathcal{D}_g}$ for some $v_{\mathcal{D}_g}\in X_{\mathcal{D}_g}$. For all $e\in\mathcal{E}_{\Sigma_{i,\Gamma}}$, we define $\underline{w}_e = \min_{x\in I_e}w(x)$ and $\overline{w}_e = \max_{x\in I_e}w(x)$ with $I_e = \{\underline{x}_e,\overline{x}_e\}\cup\{(x_m)_{m\in\mathcal{V}_\mathcal{G}} \mid \underline{x}_e < x_m < \overline{x}_e\}$. Then, reiterating the same process as for the proof of (46), we can prove that

$$\sum_{e\in\mathcal{E}_{\Sigma_{i,\Gamma}}}\|w - \sum_{\boldsymbol{s}\in\mathcal{V}_{\Sigma_\Gamma}} w(x_{\boldsymbol{s}})\mathbf{1}_{e_{\Sigma_\Gamma,\boldsymbol{s}}}\|_e^2 \le \sum_{e\in\mathcal{E}_{\Sigma_{i,\Gamma}}}|e|(\overline{w}_e - \underline{w}_e)^2 \le \sum_{e\in\mathcal{E}_{\Sigma_{i,\Gamma}}}|e|\left(\int_{\underline{x}_e}^{\overline{x}_e}|w'(x)|\mathrm{d}x\right)^2.$$

We note, in passing, that if $\underline{x}_e = \overline{x}_e$, the approximation of the trace on e is exact since $\underline{w}_e = \overline{w}_e$; see Remark 7.1. Using a Cauchy-Schwarz inequality and the fact that $|e||\overline{x}_e - \underline{x}_e| \le h_{\mathcal{M}}^2$, it holds

$$\sum_{e\in\mathcal{E}_{\Sigma_{i,\Gamma}}}\|w - \sum_{\boldsymbol{s}\in\mathcal{V}_{\Sigma_\Gamma}} w(x_{\boldsymbol{s}})\mathbf{1}_{e_{\Sigma_\Gamma,\boldsymbol{s}}}\|_e^2 \le h_{\mathcal{M}}^2\sum_{e\in\mathcal{E}_{\Sigma_{i,\Gamma}}}\int_{\underline{x}_e}^{\overline{x}_e}|w'(x)|^2\mathrm{d}x \le h_{\mathcal{M}}^2\|\nabla_{\mathcal{D}_g}v_{\mathcal{D}_g}\|_{\Omega_g}^2.$$

where we used the definition (25c) of $\nabla_{\mathcal{D}_g}$ to obtain the last bound. Finally, summing over all the fracture indices $i\in\mathcal{I}_f$ gives the expected result with $C_{\Sigma_\Gamma} = |\mathcal{I}_f|^{1/2}$. □

Remark 7.1 (Exactness on Σ_Γ)**.** *In the case where an edge $e\in\mathcal{E}_{\Sigma_\Gamma}$ is orthogonal to the tunnel, i.e., that the vertices $(\boldsymbol{x}_{\boldsymbol{s}})_{\boldsymbol{s}\in\mathcal{V}_e}$ share the same x-coordinate, one can prove that for any $v_{\mathcal{D}_g}\in X_{\mathcal{D}_g}$, it holds*

$$\|\Pi_{\mathcal{G}}v_{\mathcal{D}_g} - \sum_{\boldsymbol{s}\in\mathcal{V}_{\Sigma_\Gamma}}\Pi_{\mathcal{G}}v_{\mathcal{D}_g}(x_{\boldsymbol{s}})\mathbf{1}_{e_{\Sigma_\Gamma,\boldsymbol{s}}}\|_e = 0.$$

Indeed, in this case, denoting by $\mathcal{V}_e = \{\boldsymbol{s}_1,\boldsymbol{s}_2\}$, it holds that $(\Pi_{\mathcal{G}}v_{\mathcal{D}_g})_{|e} = \Pi_{\mathcal{G}}v_{\mathcal{D}_g}(x_{\boldsymbol{s}_1}) = \Pi_{\mathcal{G}}v_{\mathcal{D}_g}(x_{\boldsymbol{s}_2}) = \sum_{\boldsymbol{s}\in\mathcal{V}_e}\Pi_{\mathcal{G}}v_{\mathcal{D}_g}(x_{\boldsymbol{s}})\mathbf{1}_{e_{\Sigma_\Gamma,\boldsymbol{s}}\cap e}$ since $(e_{\Sigma_\Gamma,\boldsymbol{s}}\cap e)_{\boldsymbol{s}\in\mathcal{V}_e}$ forms a partition of e.

We now prove the coercivity result of the discretization $\mathcal{D}$.

Lemma 7.5 (Coercivity)**.** *The gradient discretization $\mathcal{D}$ defined by (20), (23), (25) and (27) is coercive in the sense that $C_{\mathcal{D}}$ in (11) depends only on the geometry and on the shape regularity parameter $\theta_{\mathcal{T}}$.*

Proof of Lemma 7.5. Let $\widetilde{\mathcal{D}}$ be the gradient discretization defined by (20), (24), (25) and (27). From the continuity of the trace operator γ_f, a Poincaré-Friedrichs inequality on $H^1(\Omega_m)$ and the Poincaré inequality in $H_0^1(\Omega_g)$, one has for all $v_{\mathcal{D}}\in X_{\mathcal{D}}^0$

$$\begin{aligned}\|\Pi_{\mathcal{T}}v_{\mathcal{D}_p}\|_{\Omega_m}^2 + \|\gamma_f\Pi_{\mathcal{T}}v_{\mathcal{D}_p}\|_{\Omega_f}^2 + \|\Pi_{\mathcal{G}}v_{\mathcal{D}_g}\|_{\Omega_g}^2 \lesssim \|\nabla_{\mathcal{D}_m}v_{\mathcal{D}_p}\|_{\Omega_m}^2 + \left(\int_\Gamma\gamma_\Gamma\Pi_{\mathcal{T}}v_{\mathcal{D}_p}\mathrm{d}\tau(\boldsymbol{x})\right)^2 \\ + \|\nabla_{\mathcal{D}_f}v_{\mathcal{D}_p}\|_{\Omega_f}^2 + \|\nabla_{\mathcal{D}_g}v_{\mathcal{D}_g}\|_{\Omega_g}^2.\end{aligned} \tag{47}$$

Using (26a), a Cauchy-Schwarz inequality and recalling the definition (27) of the discrete jump operator $[\![\cdot]\!]_{\mathcal{D},\Gamma}$, we get

$$\begin{aligned}\left(\int_\Gamma \gamma_\Gamma \Pi_{\mathcal{T}} v_{\mathcal{D}_p} \mathrm{d}\tau(\boldsymbol{x})\right)^2 &\le \Big(\sum_{\boldsymbol{s}\in\mathcal{V}_\Gamma} v_{\boldsymbol{s}}|\sigma_{\Gamma,\boldsymbol{s}}|\Big)^2,\\ &\le 2|\Gamma|\left(\|[\![v_{\mathcal{D}}]\!]_{\mathcal{D},\Gamma}\|_\Gamma^2 + \int_\Gamma \left|\sum_{\boldsymbol{s}\in\mathcal{V}_\Gamma} \Pi_{\mathcal{G}} v_{\mathcal{D}_g}(x_{\boldsymbol{s}})\mathbf{1}_{\sigma_{\Gamma,\boldsymbol{s}}}\right|^2 \mathrm{d}\tau(\boldsymbol{x})\right).\end{aligned} \tag{48}$$

Using that

$$\int_\Gamma \left|\sum_{\boldsymbol{s}\in\mathcal{V}_\Gamma} \Pi_{\mathcal{G}} v_{\mathcal{D}_g}(x_{\boldsymbol{s}})\mathbf{1}_{\sigma_{\Gamma,\boldsymbol{s}}}\right|^2 \mathrm{d}\tau(\boldsymbol{x}) \le \|\Pi_{\mathcal{G}} v_{\mathcal{D}_g}\|^2_{L^\infty(\Omega_g)}|\Gamma| \le \|(\Pi_{\mathcal{G}} v_{\mathcal{D}_g})'\|^2_{\Omega_g}|\Gamma|L, \tag{49}$$

it follows that

$$\left(\int_\Gamma \gamma_\Gamma \Pi_{\mathcal{T}} v_{\mathcal{D}_p} \mathrm{d}\tau(\boldsymbol{x})\right)^2 \le 2|\Gamma|\left(\|[\![v_{\mathcal{D}}]\!]_{\mathcal{D},\Gamma}\|_\Gamma^2 + \|(\Pi_{\mathcal{G}} v_{\mathcal{D}_g})'\|^2_{\Omega_g} L|\Gamma|\right). \tag{50}$$

Gathering (50) into (47) proves that $\widetilde{\mathcal{D}}$ is coercive in the sense of (11) with a constant depending only on the geometry. Finally, invoking Lemma 7.3, we obtain that $\mathcal{D}$ is also coercive in the sense of (11) with a constant depending only on the geometry and on the shape regularity parameter. □

We then prove the consistency result.

Lemma 7.6 (Consistency)**.** *For all $v \in C^\infty_{V_0^p} \times C^\infty(\overline{\Omega_g})$, there exists a constant $C_{\mathcal{S}_{\mathcal{D}}}(v) > 0$ depending on v, on the shape regularity parameter and on the geometry, such that*

$$\mathcal{S}_{\mathcal{D}}(v) \le C_{\mathcal{S}}(v)(h_{\mathcal{M}} + h_{\mathcal{G}}). \tag{51}$$

Proof of Lemma 7.6. Let $v = (v_p, v_g) \in C^\infty_{V_0^p} \times C^\infty(\overline{\Omega}_g)$. Defining $\widehat{v}_{\mathcal{D}} = (\widehat{v}_{\mathcal{D}_p}, \widehat{v}_{\mathcal{D}_g}) = \mathcal{P}_{\mathcal{D}} v = (\mathcal{P}_{\mathcal{D}_p} v_p, \mathcal{P}_{\mathcal{D}_g} v_g) \in X^0_{\mathcal{D}}$, one has using triangle inequalities

$$\begin{aligned}\mathcal{S}_{\widetilde{\mathcal{D}}}(v) \le{}& \|\nabla \Pi_{\mathcal{T}} \widehat{v}_{\mathcal{D}_p} - \nabla v_p\|_{\Omega_m} + \|\nabla_\tau \gamma_f \Pi_{\mathcal{T}} \widehat{v}_{\mathcal{D}_p} - \nabla_\tau \gamma_f v_p\|_{\Omega_f} + \|(\Pi_{\mathcal{G}} \widehat{v}_g)' - v_g'\|_{\Omega_g}\\ &+ \|\Pi_{\mathcal{T}} \widehat{v}_{\mathcal{D}_p} - v_p\|_{\Omega_m} + \|\gamma_f \Pi_{\mathcal{T}} \widehat{v}_{\mathcal{D}_p} - \gamma_f v_p\|_{\Omega_f} + \|\Pi_{\mathcal{G}} \widehat{v}_{\mathcal{D}_g} - v_g\|_{\Omega_g}\\ &+ \|[\![\widehat{v}_{\mathcal{D}}]\!]_{\mathcal{D},\Gamma} - [\![v]\!]_\Gamma\|_\Gamma + \|[\![\widehat{v}_{\mathcal{D}}]\!]_{\mathcal{D},\Sigma_\Gamma} - [\![v]\!]_{\Sigma_\Gamma}\|_{\Sigma_\Gamma}.\end{aligned} \tag{52}$$

A direct application of Lemma 7.1 with $(\varphi_p, \varphi_g) = (v_p, v_g)$ and of Lemma 7.2 with $v_{\mathcal{D}} = \widehat{v}_{\mathcal{D}}$ ensures the existence of a positive constant $C > 0$ depending on the mesh regularity parameter and v such that

$$\mathcal{S}_{\widetilde{\mathcal{D}}}(v) \le C(h_{\mathcal{M}} + h_{\mathcal{G}} + h^2_{\mathcal{M}} + h^2_{\mathcal{G}}) + \|[\![\widehat{v}_{\mathcal{D}}]\!]_{\mathcal{D},\Gamma} - [\![v]\!]_\Gamma\|_\Gamma + \|[\![\widehat{v}_{\mathcal{D}}]\!]_{\mathcal{D},\Sigma_\Gamma} - [\![v]\!]_{\Sigma_\Gamma}\|_{\Sigma_\Gamma}. \tag{53}$$

Let $\mathcal{I}_\Gamma$ and $\mathcal{I}_{\Sigma_\Gamma}$ denotes two rightmost terms on the right-hand side of (53). We first focus on $\mathcal{I}_\Gamma$. Recalling the definitions (1) and (27) of the jumps terms $[\![\cdot]\!]_\Gamma$ and $[\![\cdot]\!]_{\mathcal{D},\Gamma}$, and adding $\pm\sum_{\boldsymbol{s}\in\mathcal{V}_\Gamma} v_g(x_{\boldsymbol{s}})\mathbf{1}_{\sigma_{\Gamma,\boldsymbol{s}}}$, it holds after using triangle inequalities

$$\begin{aligned}\mathcal{I}_\Gamma \le{}& \|\gamma_\Gamma v_p - \sum_{\boldsymbol{s}\in\mathcal{V}_\Gamma} v_p(\boldsymbol{x}_{\boldsymbol{s}})\mathbf{1}_{\sigma_{\Gamma,\boldsymbol{s}}}\|_\Gamma + \|v_g - \sum_{\boldsymbol{s}\in\mathcal{V}_\Gamma} v_g(x_{\boldsymbol{s}})\mathbf{1}_{\sigma_{\Gamma,\boldsymbol{s}}}\|_\Gamma\\ &+ \|\sum_{\boldsymbol{s}\in\mathcal{V}_\Gamma} (v_g(x_{\boldsymbol{s}}) - (\Pi_{\mathcal{G}}\mathcal{P}_{\mathcal{D}_g} v_g)(x_{\boldsymbol{s}}))\mathbf{1}_{\sigma_{\Gamma,\boldsymbol{s}}}\|_\Gamma\\ \le{}& |\Gamma|^{1/2}\left(h_{\mathcal{M}}\left(\|\nabla_\tau \gamma_\Gamma v_p\|_{L^\infty(\Gamma)} + \|v_g'\|_{L^\infty(\Omega_g)}\right) + h^2_{\mathcal{G}}\|v_g''\|_{L^\infty(\Omega_g)}\right),\end{aligned} \tag{54}$$

where we used the mean value and the Rolle theorems to pass to the second line.

We now move to $\mathcal{I}_{\Sigma_\Gamma}$. Using the same arguments, one can prove that it holds

$$\begin{aligned}\mathcal{I}_{\Sigma_\Gamma} &\leq \|\gamma_{\Sigma_\Gamma}\gamma_f v_p - \sum_{\boldsymbol{s}\in\mathcal{V}_{\Sigma_\Gamma}} v_p(\boldsymbol{x}_{\boldsymbol{s}})\mathbf{1}_{e_{\Sigma_\Gamma,\boldsymbol{s}}}\|_{\Sigma_\Gamma} + \|v_g - \sum_{\boldsymbol{s}\in\mathcal{V}_{\Sigma_\Gamma}} v_g(x_{\boldsymbol{s}})\mathbf{1}_{e_{\Sigma_\Gamma,\boldsymbol{s}}}\|_{\Sigma_\Gamma} \\ &\quad + \|\sum_{\boldsymbol{s}\in\mathcal{V}_{\Sigma_\Gamma}} (v_g(x_{\boldsymbol{s}}) - (\Pi_{\mathcal{G}}\mathcal{P}_{\mathcal{D}_g}v_g)(x_{\boldsymbol{s}}))\mathbf{1}_{e_{\Sigma_\Gamma,\boldsymbol{s}}}\|_{\Sigma_\Gamma} \\ &\leq |\Sigma_\Gamma|^{1/2}\left(h_{\mathcal{M}}\left(\|(\gamma_{\Sigma_\Gamma}\gamma_f v_p)'\|_{L^\infty(\Sigma_\Gamma)} + \|v_g'\|_{L^\infty(\Omega_g)}\right) + h_{\mathcal{G}}^2\|v_g''\|_{L^\infty(\Omega_g)}\right).\end{aligned} \tag{55}$$

Finally, gathering (54) and (55) into (53) and applying Lemma 7.3, (51) follows. □

Finally, we prove the limit conformity result.

Lemma 7.7 (Limit conformity)**.** *For all $\boldsymbol{w} \in C_W^\infty$, there exists a constant $C_{\mathcal{W}}(\boldsymbol{w}) > 0$ depending only on $\boldsymbol{w}$, the geometry and on the mesh regularity parameter such that*

$$\mathcal{W}_{\mathcal{D}}(\boldsymbol{w}) \leq C_{\mathcal{W}}(\boldsymbol{w})(h_{\mathcal{M}} + h_{\mathcal{G}}). \tag{56}$$

Proof of Lemma 7.7. Let $W_{\widetilde{\mathcal{D}}} : C_W^\infty \times X_{\mathcal{D}}^0 \to \mathbb{R}$ be such that, for all $\boldsymbol{w} = (\boldsymbol{w}_m, \boldsymbol{w}_f, w_g) \in C_W^\infty$ and $v_{\mathcal{D}} = (v_{\mathcal{D}_p}, v_{\mathcal{D}_g}) \in X_{\mathcal{D}}^0$,

$$\begin{aligned}W_{\widetilde{\mathcal{D}}}(\boldsymbol{w}, v_{\mathcal{D}}) &= \int_{\Omega_m} \boldsymbol{w}_m \cdot \nabla_{\mathcal{D}_m} v_{\mathcal{D}_p} + \Pi_{\mathcal{T}} v_{\mathcal{D}_p}\ \mathrm{div}(\boldsymbol{w}_m)\mathrm{d}\boldsymbol{x} + \int_{\Omega_f} \boldsymbol{w}_f \cdot \nabla_{\mathcal{D}_f} v_{\mathcal{D}_p} + \gamma_f \Pi_{\mathcal{T}} v_{\mathcal{D}_p}\ r_f(\boldsymbol{w})\mathrm{d}\tau(\boldsymbol{x}) \\ &\quad + \int_{\Omega_g} w_g \nabla_{\mathcal{D}_g} v_{\mathcal{D}_g} + \Pi_{\mathcal{G}} v_{\mathcal{D}_g}\ r_g(\boldsymbol{w})\mathrm{d}l(\boldsymbol{x}) - \int_\Gamma (\boldsymbol{w}_m \cdot \boldsymbol{n}_\Gamma)[\![v_{\mathcal{D}}]\!]_{\mathcal{D},\Gamma}\mathrm{d}\tau(\boldsymbol{x}) \\ &\quad - \int_{\Sigma_\Gamma} (\boldsymbol{w}_f \cdot \boldsymbol{n}_{\Sigma_\Gamma})[\![v_{\mathcal{D}}]\!]_{\mathcal{D},\Sigma_\Gamma}\mathrm{d}l(\boldsymbol{x}).\end{aligned} \tag{57}$$

Recalling the definition (5) of the space C_W^∞ together with the definition (27) of the jump terms $[\![\cdot]\!]_{\mathcal{D},\Gamma}$ and $[\![\cdot]\!]_{\mathcal{D},\Sigma_\Gamma}$, it holds for any $\boldsymbol{w} = (\boldsymbol{w}_m, \boldsymbol{w}_f, w_g) \in C_W^\infty$ and $v_{\mathcal{D}} \in X_{\mathcal{D}}^0$,

$$\begin{aligned}W_{\widetilde{\mathcal{D}}}(\boldsymbol{w}, v_{\mathcal{D}}) &= \sum_{\sigma\in\mathcal{F}_\Gamma} \int_\sigma (\boldsymbol{w}_m \cdot \boldsymbol{n}_\Gamma)(\gamma_\Gamma \Pi_{\mathcal{T}} v_{\mathcal{D}_p} - \sum_{\boldsymbol{s}\in\mathcal{V}_\Gamma} v_{\boldsymbol{s}}\mathbf{1}_{\sigma_{\Gamma,\boldsymbol{s}}})\mathrm{d}\tau(\boldsymbol{x}) \\ &\quad + \sum_{e\in\mathcal{E}_{\Sigma_\Gamma}} \int_e (\boldsymbol{w}_f \cdot \boldsymbol{n}_{\Sigma_\Gamma})(\gamma_{\Sigma_\Gamma}\gamma_f \Pi_{\mathcal{T}} v_{\mathcal{D}_p} - \sum_{\boldsymbol{s}\in\mathcal{V}_{\Sigma_\Gamma}} v_{\boldsymbol{s}}\mathbf{1}_{e_{\Sigma_\Gamma,\boldsymbol{s}}})\mathrm{d}l(\boldsymbol{x}) \\ &\quad + \sum_{\sigma\in\mathcal{F}_\Gamma} \int_\sigma (\boldsymbol{w}_m \cdot \boldsymbol{n}_\Gamma)(\sum_{\boldsymbol{s}\in\mathcal{V}_\Gamma} \Pi_{\mathcal{G}} v_{\mathcal{D}_g}(x_{\boldsymbol{s}})\mathbf{1}_{\sigma_{\Gamma,\boldsymbol{s}}} - \Pi_{\mathcal{G}} v_{\mathcal{D}_g})\mathrm{d}\tau(\boldsymbol{x}) \\ &\quad + \sum_{e\in\mathcal{E}_{\Sigma_\Gamma}} \int_e (\boldsymbol{w}_f \cdot \boldsymbol{n}_{\Sigma_\Gamma})(\sum_{\boldsymbol{s}\in\mathcal{V}_{\Sigma_\Gamma}} \Pi_{\mathcal{G}} v_{\mathcal{D}_g}(x_{\boldsymbol{s}})\mathbf{1}_{e_{\Sigma_\Gamma,\boldsymbol{s}}} - \Pi_{\mathcal{G}} v_{\mathcal{D}_g})\mathrm{d}l(\boldsymbol{x}) \\ &=: \mathcal{I}_1 + \mathcal{I}_2 + \mathcal{I}_3 + \mathcal{I}_4.\end{aligned} \tag{58}$$

We first focus on $\mathcal{I}_1$ and $\mathcal{I}_2$. Setting $\mathrm{w}_m^\sigma = |\sigma|^{-1}\int_\sigma \boldsymbol{w}_m \cdot \boldsymbol{n}_\Gamma \mathrm{d}\tau(\boldsymbol{x})$ (resp. $\mathrm{w}_f^e = |e|^{-1}\int_e \boldsymbol{w}_f \cdot \boldsymbol{n}_{\Sigma_\Gamma}\mathrm{d}l(\boldsymbol{x})$) for all $\sigma \in \mathcal{F}_\Gamma$ (resp. on e for all $e \in \mathcal{E}_{\Sigma_\Gamma}$), recalling the definitions (26a) and

(26b), one has that

$$\int_\sigma \mathrm{w}_m^\sigma \left(\gamma_\Gamma \Pi_{\mathcal{T}} v_{\mathcal{D}_p} - \sum_{\boldsymbol{s}\in\mathcal{V}_\Gamma} v_{\boldsymbol{s}} \mathbf{1}_{\sigma_\Gamma,\boldsymbol{s}} \right) \mathrm{d}\tau(\boldsymbol{x}) = 0 \qquad \forall \sigma \in \mathcal{F}_\Gamma, \tag{59a}$$

$$\int_e \mathrm{w}_f^e \left(\gamma_{\Sigma_\Gamma} \gamma_f \Pi_{\mathcal{T}} v_{\mathcal{D}_p} - \sum_{\boldsymbol{s}\in\mathcal{V}_{\Sigma_\Gamma}} v_{\boldsymbol{s}} \mathbf{1}_{e_{\Sigma_\Gamma},\boldsymbol{s}} \right) \mathrm{d}l(\boldsymbol{x}) = 0 \qquad \forall e \in \mathcal{E}_{\Sigma_\Gamma}. \tag{59b}$$

Subtracting (59a) for all $\sigma \in \mathcal{F}_\Gamma$ to $\mathcal{I}_1$ (resp. (59b) for all $e \in \mathcal{E}_{\Sigma_\Gamma}$ to $\mathcal{I}_2$) followed by a Cauchy-Schwarz inequality, it holds

$$\begin{aligned}\mathcal{I}_1 + \mathcal{I}_2 \le &\left(\sum_{\sigma\in\mathcal{F}_\Gamma} \|\boldsymbol{w}_m \cdot \boldsymbol{n}_\Gamma - \mathrm{w}_m^\sigma\|_\sigma^2 \right)^{1/2} \left(\sum_{\sigma\in\mathcal{F}_\Gamma} \|\gamma_\Gamma \Pi_{\mathcal{T}} v_{\mathcal{D}_p} - \sum_{\boldsymbol{s}\in\mathcal{V}_\Gamma} v_{\boldsymbol{s}} \mathbf{1}_{\sigma_\Gamma,\boldsymbol{s}}\|_\sigma^2 \right)^{1/2} \\ &+ \left(\sum_{e\in\mathcal{E}_{\Sigma_\Gamma}} \|\boldsymbol{w}_f \cdot \boldsymbol{n}_{\Sigma_\Gamma} - \mathrm{w}_f^e\|_e^2 \right)^{1/2} \left(\sum_{e\in\mathcal{E}_{\Sigma_\Gamma}} \|\gamma_{\Sigma_\Gamma}\gamma_f \Pi_{\mathcal{T}} v_{\mathcal{D}_p} - \sum_{\boldsymbol{s}\in\mathcal{V}_{\Sigma_\Gamma}} v_{\boldsymbol{s}} \mathbf{1}_{e_{\Sigma_\Gamma},\boldsymbol{s}}\|_e^2 \right)^{1/2}.\end{aligned} \tag{60}$$

Using a Poincaré-Wirtinger inequality on σ for all $\sigma \in \mathcal{F}_\Gamma$ (resp. all $e \in \mathcal{E}_{\Sigma_\Gamma}$), we infer the existence of $C_{1,\boldsymbol{w}_m} > 0$ (resp. $C_{2,\boldsymbol{w}_f} > 0$) depending on $\boldsymbol{w}_m$ (resp. $\boldsymbol{w}_f$) such that

$$\sum_{\sigma\in\mathcal{F}_\Gamma} \|\boldsymbol{w}_m \cdot \boldsymbol{n}_\Gamma - \mathrm{w}_m^\sigma\|_\sigma^2 \le C_{1,\boldsymbol{w}_m} h_{\mathcal{M}}^2, \quad \sum_{e\in\mathcal{E}_{\Sigma_\Gamma}} \|\boldsymbol{w}_f \cdot \boldsymbol{n}_{\Sigma_\Gamma} - \mathrm{w}_f^e\|_e^2 \le C_{2,\boldsymbol{w}_f} h_{\mathcal{M}}^2. \tag{61}$$

The two remaining terms in the right-hand side of (60) are bounded as follows. Let $\sigma \in \mathcal{F}_\Gamma$, $\kappa \in \mathcal{M}_\sigma$ and $v = \Pi_{\mathcal{T}} v_{\mathcal{D}_p}$. Setting $\underline{v}_\sigma = \min_{\boldsymbol{s}\in\mathcal{V}_\sigma} v(\boldsymbol{x}_{\boldsymbol{s}})$ and $\overline{v}_\sigma = \max_{\boldsymbol{s}\in\mathcal{V}_\sigma} v(\boldsymbol{x}_{\boldsymbol{s}})$, it holds

$$\begin{aligned}\|\gamma_\Gamma v - \sum_{\boldsymbol{s}\in\mathcal{V}_\Gamma} v(\boldsymbol{x}_{\boldsymbol{s}}) \mathbf{1}_{\sigma_\Gamma,\boldsymbol{s}}\|_\sigma^2 &\le |\sigma|(\overline{v}_\sigma - \underline{v}_\sigma)^2 \lesssim h_\kappa^4 \left(\sum_{\boldsymbol{s}\in\mathcal{V}_\sigma} \frac{|v(\boldsymbol{x}_{\boldsymbol{s}}) - v(\boldsymbol{x}_\kappa)|}{h_\kappa} \right)^2 \\ &\lesssim h_{\mathcal{M}} |\mathcal{V}_\sigma| |\kappa| \sum_{\boldsymbol{s}\in\mathcal{V}_\kappa} \frac{(v(\boldsymbol{x}_{\boldsymbol{s}}) - v(\boldsymbol{x}_\kappa))^2}{h_\kappa^2} \lesssim h_{\mathcal{M}} \|\nabla_{\mathcal{D}_m} v_{\mathcal{D}_p}\|_\kappa^2,\end{aligned} \tag{62}$$

where we used the fact that $|\sigma| \lesssim h_\kappa^2$ to pass to the second inequality, a Cauchy-Schwarz inequality together with the fact that $h_\kappa^4 \lesssim h_{\mathcal{M}}|\kappa|$ to pass to the second line, and [9, Lemma 3.2] to conclude. In (62), all the hidden constants depend on the mesh regularity parameter. We now let $e \in \mathcal{E}_{\Sigma_\Gamma}$ and $\sigma \in \mathcal{F}_e \cap \mathcal{F}_f$. Using the same arguments as for (62), one can prove

$$\|\gamma_{\Sigma_\Gamma} v - \sum_{\boldsymbol{s}\in\mathcal{V}_{\Sigma_\Gamma}} v(\boldsymbol{x}_{\boldsymbol{s}}) \mathbf{1}_{e_{\Sigma_\Gamma},\boldsymbol{s}}\|_e^2 \lesssim h_{\mathcal{M}} \|\nabla_{\mathcal{D}_f} v_{\mathcal{D}_p}\|_\sigma^2, \tag{63}$$

Also in (63), all the hidden constants depend on the mesh regularity parameter. Combining (61), (62) and (63) into (60), it follows

$$\mathcal{I}_1 + \mathcal{I}_2 \lesssim h_{\mathcal{M}}^{3/2} \left(\|\nabla_{\mathcal{D}_m} v_{\mathcal{D}_p}\|_{\Omega_m} + \|\nabla_{\mathcal{D}_f} v_{\mathcal{D}_p}\|_{\Omega_f} \right), \tag{64}$$

with hidden constant inheriting previous dependencies. For $\mathcal{I}_3$ and $\mathcal{I}_4$, using a Cauchy-Schwarz inequality together with Lemma 7.4 allow us to infer

$$\mathcal{I}_3 + \mathcal{I}_4 \lesssim h_{\mathcal{M}} \|\nabla_{\mathcal{D}_g} v_{\mathcal{D}_g}\|_{\Omega_g}, \tag{65}$$

where the hidden constant has the same dependencies as in Lemma 7.4. Using (64) and (65) in (58) gives

$$W_{\widetilde{\mathcal{D}}}(\boldsymbol{w}, v_{\mathcal{D}}) \lesssim h_{\mathcal{M}} \left(\|\nabla_{\mathcal{D}_m} v_{\mathcal{D}_p}\|_{\Omega_m} + \|\nabla_{\mathcal{D}_f} v_{\mathcal{D}_p}\|_{\Omega_f} + \|\nabla_{\mathcal{D}_g} v_{\mathcal{D}_g}\|_{\Omega_g} \right). \tag{66}$$

Recalling the definition (10) of the $\|\cdot\|_{\mathcal{D}}$-norm and taking the supremum over all $v_{\mathcal{D}} \in X^0_{\mathcal{D}} \backslash \{0\}$ gives $\mathcal{W}_{\widetilde{\mathcal{D}}}(\boldsymbol{w}) \lesssim h_{\mathcal{M}}$ from which (56) is deduced using Lemma 7.3. □

Proof of Proposition 4.1. It derives from Lemmae 7.5, 7.6, 7.7 and from the density results of Lemmae 2.1 and 2.2. □

Proof of Proposition 4.2. It is deduced from Theorem 3.2 and from the proofs of Lemmae 7.6, 7.7 showing that the first order estimates still hold for matrix cell-wise, fracture face-wise and tunnel cell-wise smooth solutions. □

References

[1] C. Alboin, J. Jaffré, J. E. Roberts, and C Serres. Modeling fractures as interfaces for flow and transport in porous media. In Z. Chen and R. E. Ewing, editors, Fluid flow and transport in porous media: mathematical and numerical treatment (South Hadley, MA, 2001), number 295 in Contemp. Math., pages 13–24. Amer. Math. Soc., Providence, RI, 2002.

[2] C. Alboin, J. Jaffré, J. E. Roberts, and C. Serres. Modeling fractures as interfaces for flow and transport in porous media. In Z. Chen and E. E. Richard, editors, Fluid Flow and Transport in Porous Media: Mathematical and Numerical Treatment, number 295 in Amer. Math. Soc., Providence, RI, pages 13–24. Contemp. Math., 2002.

[3] P. Angot, F. Boyer, and F. Hubert. Asymptotic and numerical modeling of flows in fractured porous media. ESAIM: M2AN, 43(2):239–275, 2009.

[4] K. Baber, K. Mosthaf, B. Flemisch, R. Helmig, and S. Müthing. Numerical scheme for coupling two-phase compositional porous-media flow and one-phase compositional free flow. IMA J. Numer. Anal., 77(6):887–909, 2012.

[5] S. Berrone, D. Grappein, and S. Scialó. 3D-1D coupling on non conforming meshes via a three-field optimization based domain decomposition. J. Comput. Phys., 448:110738, 2022.

[6] I. Bogdanov, V. Mourzenko, J. F. Thovert, and P. M. Adler. Two-phase flow through fractured porous media. Phys. Rev. E Stat. Nonlin. Soft. Matter Phys., 68(2 Pt 2):026703, 2003.

[7] K. Brenner, M. Groza, C. Guichard, G. Lebeau, and R. Masson. Gradient discretization of hybrid-dimensional darcy flows in fractured porous media. Numer. Math., 134:569–609, 2016.

[8] K. Brenner, J. Hennicker, R. Masson, and P. Samier. Gradient discretization of hybrid-dimensional darcy flow in fractured porous media with discontinuous pressures at matrix-fracture interfaces. IMA J. Numer. Anal., 37(3):1551–1585, 2016.

[9] K. Brenner and R. Masson. Convergence of a vertex centred discretization of two-phase darcy flows on general meshes. Int. J. Finite Vol., 10:1–37, 2013.

[10] K. Brenner, R. Masson, L. Trenty, and Y. Zhang. Coupling of a two phase gas liquid compositional 3D darcy flow with a 1D compositional free gas flow. ESAIM: M2AN, 50(5):1491–1522, 2016.

[11] F. Brezzi, K. Lipnikov, and Simoncini V. A family of mimetic finite difference methods on polygonal and polyhedral meshes. Math. Models Methods Appl. Sci., 46(2):1533–1552, 2005.

[12] L. Cattaneo and P. Zunino. Computational models for fluid exchange between microcirculation and tissue interstitium. Netw. Heterog. Media, 9(1):135–159, 2014.

[13] D. Cerroni, F. Laurino, and P. Zunino. Mathematical analysis, finite element approximation and numerical solvers for the interaction of 3D reservoirs with 1D wells. GEM Int. J. Geomath., 10(4), 2019.

[14] C. D'Angelo. Finite Element approximation of elliptic problems with Dirac measure terms in weighted spaces: Applications to one- and three-dimensional coupled problems. SIAM J. Numer. Anal., 50(1):194–215, 2012.

[15] C. D'Angelo and A. Quarteroni. On the coupling of 1D and 3D diffusion-reaction equations: application to tissue perfusion problems. Math. Models Methods Appl. Sci., 18(8):1481–1504, 2008.

[16] T. Defraeye. Advanced computational modelling for drying processes – A review. Appl. Energy, 131(15):323–344, 2014.

[17] J. Droniou, R. Eymard, T. Gallouët, C. Guichard, and R. Herbin. The gradient discretisation method, volume 82 of Mathematics & Applications. Springer International Publishing, 2018.

[18] J. Droniou, R. Eymard, T. Gallouet, and R. Herbin. A unified approach to mimetic finite difference, hybrid finite volume and mixed finite volume methods. Math. Models Methods Appl. Sci., 20(2):265–295, 2010.

[19] J. Droniou, R. Eymard, and R. Herbin. Gradient schemes: generic tools for the numerical analysis of diffusion equations. ESAIM: M2AN, 50(3):749–781, 2016.

[20] C. Engwer, J. Vorwerk, J. Ludewig, and C. H. Wolters. A discontinuous galerkin method to solve the EEG forward problem using the subtraction approach. SIAM J. Sci. Comput., 39(1):B138–B164, 2017.

[21] A. Ern and J. L. Guermond. Theory and Practice of Finite Elements, volume 159 of Applied Mathematical Sciences. Springer-Verlag New York, 2004.

[22] R. Eymard, T. Gallouët, and R. Herbin. Discretisation of heterogeneous and anisotropic diffusion problems on general nonconforming meshes sushi: a scheme using stabilisation and hybrid interfaces. IMA J. Numer. Anal., 30(4):1009–1043, 2010.

[23] R. Eymard, C. Guichard, and R. Herbin. Small-stencil 3D schemes for diffusive flows in porous media. ESAIM: M2AN, 46(2):265–290, 2010.

[24] E. Flauraud, F. Nataf, I. Faille, and R. Masson. Domain decomposition for an asymptotic geological fault modeling. C. R. Mecanique, 331:849–855, 2003.

[25] M. Fritz, P. K. Jha, T. Köppl, J. T. Oden, A. Wagner, and B. Wohlmuth. Modeling and simulation of vascular tumors embedded in evolving capillary networks. Comput. Methods Appl. Mech. Engrg., 384:113975, 2021.

[26] M. Fritz, P. K. Jha, T. Köppl, J. T. Oden, and B. Wohlmuth. Analysis of a new multispecies tumor growth model coupling 3D phase-fields with a 1D vascular network. Nonlinear Anal. RWA., 61:103331, 2021.

[27] I. G. Gjerde, K. Kumar, and J. M. Nordbotten. Well modelling by means of coupled 1D-3D flow models. In European Association of Geoscientists & Engineers, editor, ECMOR XVI – 16th European Conference on the Mathematics of Oil Recovery, pages 1–12, 2018.

[28] I. G. Gjerde, K. Kumar, J. M. Nordbotten, and B. Wohlmuth. Splitting method for elliptic equations with line sources. ESAIM: M2AN, 53(5):1715–1739, 2019.

[29] R. Hsu and T. W. Secomb. A green's function method for analysis of oxygen delivery to tissue by microvascular networks. Math. Biosci., 96(1):61–78, 1989.

[30] J. Jaffré, V. Martin, , and J. E. Roberts. Modeling fractures and barriers as interfaces for flow in porous media. SIAM J. Sci. Comput., 26(5):1667–1691, 2005.

[31] M. Javaux, T. Schröder, J. Vanderborght, and H. Vareecken. Use of a three-dimensional detailed modeling approach for predicting root water uptake. Vadose Zone J., 7(3):1079–1088, 2008.

[32] M. Karimi-Fard, L. J. Durlofsky, and K. Aziz. An efficient discrete-fracture model applicable for general-purpose reservoir simulators. Soc. Pet. Eng. J., 9(2):227–236, 2004.

[33] T. Koch. Projection-based resolved interface mixed-dimension method for embedded tubular network systems, 2021. Submitted.

[34] T. Koch, K. Heck, N. Schröder, H. Class, and R. Helmig. A new simulation framework for soil-root interaction, evaporation, root growth, and solute transport. Vadose Zone J., 17(1):1–21, 2018.

[35] T. Koch, M. Schneider, R. Helmig, and P. Jenny. Modeling tissue perfusion in terms of 1D-3D embedded mixed-dimension coupled problems with distributed sources. J. Comput. Phys., 410:109370, 2020.

[36] T. Koch, H. Wu, and M. Schneider. Nonlinear mixed-dimension model for embedded tubular networks with application to root water uptake, 2021. Submitted.

[37] T/ Köppl, E. Vidotto, and B. Wohlmuth. A 3D-1D coupled blood flow and oxygen transport model to generate microvascular networks. Int. J. Numer. Meth. Biomed. Engng., 36(10):e3386, 2020.

[38] T. Köppl, E. Vidotto, B. Wohlmuth, and P. Zunino. Mathematical modeling, analysis and numerical approximation of second-order elliptic problems with inclusions. Math. Models Methods Appl. Sci., 28(5):953–978, 2018.

[39] F. Laurino and P. Zunino. Derivation and analysis of coupled PDEs on manifolds with high dimensionality gap arising from topological model reduction. ESAIM: M2AN, 53(6):2047–2080, 2019.

[40] A. Llau, L. Jason, F. Dufour, and J. Baroth. Finite element modelling of 1D steel components in reinforced and prestressed concrete structures. Eng. Struct., 127:769–783, 2016.

[41] K. Mosthaf, K. Baber, B. Flemisch, R. Helmig, A. Leijnse, I. Rybak, and B. Wohlmuth. A coupling concept for two-phase compositional porous-medium and single-phase compositional free flow. Water Resour. Res., 47(10):W10522, 2011.

[42] J. M. Nordbotten, W. M. Boon, A. Fumagalli, and E. Keilegavlen. Unified approach to discretization of flow in fractured porous media. Comput. Geosci., 23:225–237, 2019.

[43] D. Notaro, L. Cattaneo, L. Formaggia, A. Scotti, and P. Zunino. A mixed finite element method for modeling the fluid exchange between microcirculation and tissue interstitium. In G. Ventura and E. Benvenuti, editors, Advances in Discretization Methods, number 12 in SEMA SIMAI, pages 3–25. Springer, 2016.

[44] M. S. Olufsen and A. Nadim. On deriving lumped models for blood flow and pressure in the systemic arteries. Math. Biosci. Eng., 1(1):61–80, 2004.

[45] V. Reichenberger, H. Jakobs, P. Bastian, and R. Helmig. A mixed-dimensional finite volume method for multiphase flow in fractured porous media. Adv. Water Res., 29(7):1020–1036, 2006.

[46] L. R. Scott and S. Zhang. Finite element interpolation of non-smoothed functions satisfying boundary conditions. Mathematics of Computation, 54(190):483–493, 1990.

[47] J. Vanderborght, T. Fetzer, K. Mosthaf, K.M. Smits, and R. Helmig. Heat and water transport in soils and across the soil-atmosphere interface: 1. theory and different model concepts. Water Resour. Res., 53(2):1057–1079, 2017.

[48] E. Vidotto, T. Koch, T. Köppl, R. Helmig, and B. Wohlmuth. Hybrid models for simulating blood flow in microvascular networks. Multiscale Model. Simul., 17(3):1076–1102, 2019.

[49] Y. Zhang. Modelling and simulation of ventilation devices in nuclear waste geological repositories. PhD thesis, Université Nice Sophia Antipolis, 2015.